APPLYING FREQUENCY-DOMAIN EQUALIZATION
TO
CODE-DIVISION MULTIPLE ACCESS
AND
TRANSFORM-DOMAIN COMMUNICATIONS SYSTEMS

THESIS

ALFRED A. TAMAYO, III, Captain, USAF

AFIT/GE/ENG/08-33

DEPARTMENT OF THE AIR FORCE
AIR UNIVERSITY

AIR FORCE INSTITUTE OF TECHNOLOGY

Wright-Patterson Air Force Base, Ohio

AFIT/GE/ENG/08-33

Applying Frequency-Domain Equalization
to
Code-Division Multiple Access
and
Transform-Domain Communications Systems

THESIS

Presented to the Faculty

Department of Electrical and Computer Engineering

Graduate School of Engineering and Management

Air Force Institute of Technology

Air University

Air Education and Training Command

In Partial Fulfillment of the Requirements for the

Degree of Master of Science in Electrical Engineering

ALFRED A. TAMAYO, III, BS, MBA

Captain, USAF

March 2008

Applying Frequency-Domain Equalization
to
Code-Division Multiple Access
and
Transform-Domain Communications Systems

ALFRED A. TAMAYO, III, BS, MBA

Captain, USAF

Approved:

/signed/	29 Mar 2008
Dr. Richard K. Martin (Chairman)	date
/signed/	29 Mar 2008
Dr. Michael A. Temple (Member)	date
/signed/	29 Mar 2008
Dr. Robert F. Mills (Member)	date

Abstract

This research examined the theory and application of using orthogonal frequency division multiplexing (OFDM), or discrete multi-tone (DMT), frequency-domain equalization (FEQ) with two communications systems that inherently possess unused carrier frequencies, or null-tones, in their respective transmission frequencies. The fundamental DMT-FEQ property relies on null-tones to equalize a non-ideal channel and mitigate the effects of interchannel interference (ICI), intersymbol interference (ISI), and noise. The two communications systems investigated were a Hadamard encoded code division multiple access (CDMA) communications system with up to 32 synchronous users and a transform domain communications system (TDCS) with only one user. Both communications systems were simulated while operating with real channel data corrupted by noise.

Simulation results showed that the Hadamard encoded CDMA system worked well with DMT-FEQ only when the Hadamard code set was used to construct a transmission signal that obeyed DMT-FEQ null-tone conditions in conjunction with a vector estimation method. Simulation results also showed that a TDCS using traditional pseudo-random phase component, and traditional spectral mask with consecutive null-tones, did not work well with DMT-FEQ. Modifications to the TDCS model revealed that a TDCS with a conjugate-symmetric phase component in conjunction with a modified spectral mask with consecutive null-tones and forced null-tones provided acceptable results when equalizing with DMT-FEQ. The DMT-FEQ may be suitable for covert applications, such as TDCS, when modifications to TDCS' phase component and forced null-tones in its spectral mask are made.

Acknowledgements

First and foremost, this thesis is dedicated to two of my close family members who have passed away. My late grandfather who passed away while I was flying over the Pacific Ocean trying to make it back home to see him and my late cousin who was only three months older than me and recently passed away on Christmas 2007. Although my cousin and I both parted ways on not the best of terms the last time we spoke, I can say without a doubt that he was my favorite cousin. You are both missed, always....

I want to thank my wife for her understanding and compassion when AFIT required me to spend a majority of my time studying, taking tests, writing reports, and working on my thesis. I also want to thank Dr. Richard Martin for guiding me through my research and not allowing me to get too frustrated over the many minor errors I made along the way.

Finally, I want to thank the United States Air Force for all my experiences as an officer in the world's best Air Force. My first assignment in Misawa, Japan provided me with culture broadening experiences that are critical in today and tomorrow's global economy. My second assignment was with the 3d Combat Communications Group, A.K.A. the 3d Herd, and provided me with invaluable experiences working with tactical communications equipment and combat communicators. Being in the Herd also gave me the unique opportunity to become a proud member of the Wolfpack and train the new 3d Herd members to become combat communicators, which I thoroughly enjoyed and definitely recommend to anybody. Pack out!

ALFRED A. TAMAYO, III

Table of Contents

List of Figures

List of Symbols

List of Abbreviations

xiii

Applying Frequency-Domain Equalization

to

Code-Division Multiple Access

and

Transform-Domain Communications Systems

I. Introduction

1.1 Background

The discrete-multitone (DMT) frequency-domain equalizer (FEQ) was introduced as an alternative to existing asymmetric digital subscriber line (ADSL) equalization techniques in order to decrease the latency effects of equalization in the time-domain [20–22]. The DMT-FEQ is not classified as a blind equalizer since it relies on a channel identification and used carrier frequencies and null-tones. The DMT-FEQ was implemented in this research effort due to its authors' claims of its ability to perfectly equalize a channel to remove interchannel interference (ICI) and intersymbol interference (ISI) in a communications system that possesses unused carrier frequencies, or null-tones. Two communications systems that inherently possess null-tones are a Hadamard encoded code-division multiple access (CDMA) communications systems and transform-domain communications systems (TDCS).

CDMA techniques were first introduced in military applications during World War II [14]. Currently, CDMA is used by both military and civilian applications around the globe. TDCS is designed for military applications that require low probability of detection (LPD) and low probability of intercept (LPI).

1.2   Problem Statement

The primary objective of this research effort was to combine a Hadamard encoded CDMA communications system with the DMT-FEQ described in [20–22]. The secondary objective was the use of DMT-FEQ in LPD/LPI military applications, such as TDCS.

1.3   Assumptions

Three major assumptions were made in order to progress through this research in a realistic and timely fashion: the channel data that was used was time invariant and was also shortened to maintain compatibility with the DMT-FEQ (described in section 3.1.1), the noise inserted into the receiver in the simulations was Gaussian, and the noise used in the simulations involving the first half of the Hadamard spreading code set, $\mathbf{h}_{1:32}$, was assumed to be zero-mean with unit variance in order to construct an invertible noise covariance matrix. Also, the channel was assumed to be known exactly.

1.4   Methodology

The methodology employed in this research effort explored two communications systems, Hadamard encoded CDMA and TDCS, that inherently possess null-tones in their respective transmission carrier frequencies, used in conjunction with the DMT-FEQ. With respect to the Hadamard encoded CDMA system, intricacies of the transmitter, properties of the DMT-FEQ, impact of equalizing received signals with the DMT-FEQ, derivations of both the scalar and vector maximum likelihood estimates (MLE), and the requirement for a post-estimation decision function were all thoroughly explored. And, with respect to the TDCS model, incremental changes in the spectral mask and the phase component was conducted in order to try to identify non-compatibility issues with the DMT-FEQ and a traditional TDCS system.

1.5 *Materials*

The following materials were vital to this research effort: Dell Precision 380 desktop computer with MATLAB version 7.4.0.287 (R2007a) for simulations.

1.6 *Overview*

Chapter one is the introduction. Chapter two reviews existing, relevant material to the research presented in this thesis and is intended to provide the reader with a thorough frame of reference for the proceeding material. Chapter three describes the implementation of the DMT-FEQ in conjunction with two different types of communications system models that inherently possess null-tones in their respective transmission carrier frequencies. Chapter four describes simulation results of equalizing a Hadamard encoded CDMA communications system and a TDCS with the DMT-FEQ. Chapter five concludes this research effort.

II. Literature Review

The research presented in this thesis involves the discrete-multitone (DMT), also known as orthogonal frequency division multiplexing (OFDM) frequency-domain equalizer (FEQ) used in conjunction with communication systems that inherently possess null-tones in their respective transmission signals. Therefore, in order to provide a solid frame of reference for the research presented in this thesis, the following areas of signal processing and communications will be briefly reviewed: DMT-FEQ, code-division multiple access (CDMA) communications systems, quadrature phase shift keying (QPSK), quadrature amplitude modulation (QAM), and transform-domain communications systems (TDCS).

2.1 Discrete-Multitone Frequency-Domain Equalization

The communications systems used in the simulations were modeled with the DMT-FEQ as described in [20–22]. The DMT-FEQ achieves signal reconstruction by utilizing samples from normally unused carriers, or null-tones, to equalize inter-channel interference (ICI) and intersymbol interference (ISI). The DMT-FEQ is not classified as a blind equalizer since it relies on a channel identification and used carrier frequencies and null-tones.

DMT-FEQ signal reconstruction can be achieved as long as either of the two-case null-tone rules and the equidistant null-tone rule noted in [20–22] are not violated. These null-tone rules state that case 1 is $K \geq L_c - 1, L_c - 1 < 2N$, case 2 is $K \geq 2N, L_c - 1 \geq 2N$, and the equidistant null-tone rule requires $\frac{M}{K} - 1$ used carrier frequencies between each null-tone, where K denotes the total number of null-tones present, L_c is the length of the channel impulse response (CIR), and N is the total number of the communications system's used carrier frequencies.

The simulation results noted in [20–22] primarily focused on an OFDM system's performance with respect to its data rate (Kbps) versus its introduced redundancy ($\frac{CP}{K}$), where CP denotes the length of the cyclic prefix. The simulations noted in
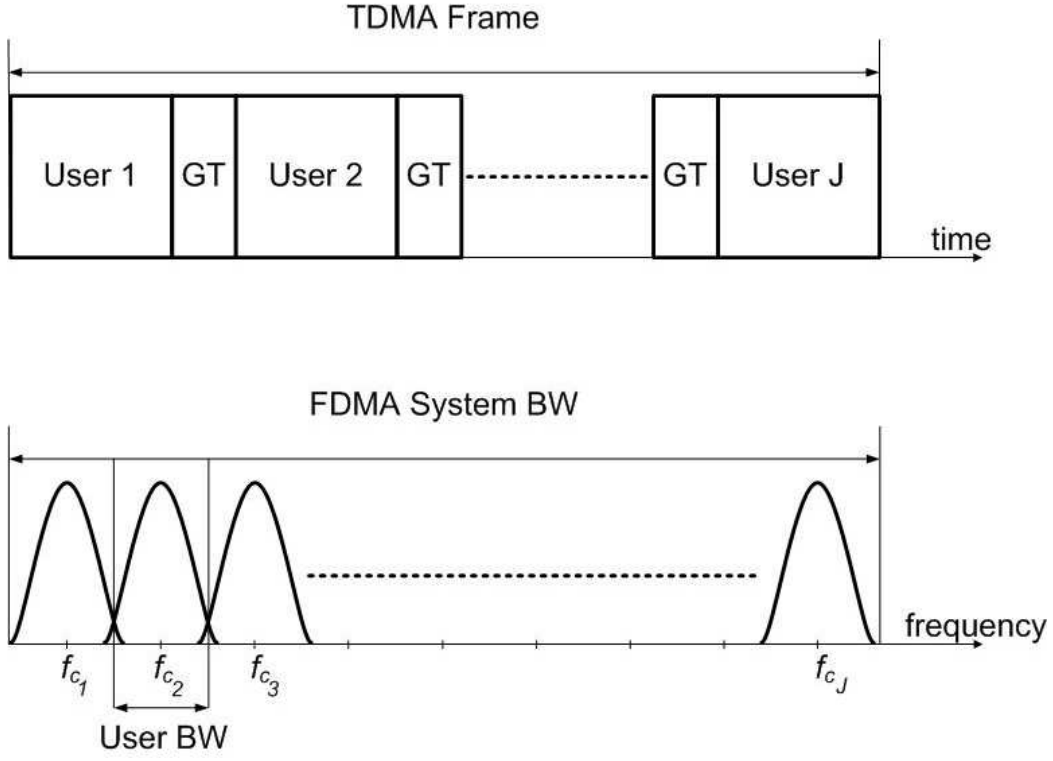
Figure 2.1:   TDMA users are restricted to individual time slots to transmit and receive data. Typically, guard time (GT) is used in TDMA systems to prevent inter-user interference. FDMA users are restricted to individual carrier frequencies, f_c, to transmit and receive data.

[20–22] maximized an OFDM system's data rates for a given probability of bit errors, P_b. See Fig. 8 of [21].

2.2   Code-Division Multiple Access Communications Systems

Communications systems that employ CDMA are also referred to as spread spectrum multiple access communications systems due to their ability of allowing multiple signals to simultaneously occupy the same radio frequency (RF) bandwidth without interfering with one another [14, 19]. CDMA does not have restrictions on time or bandwidth that time-division multiple access (TDMA) or frequency-division multiple access (FDMA), respectively possess. As shown in Fig. 2.1, users of TDMA communications systems and FDMA communications systems are restricted on time and

5
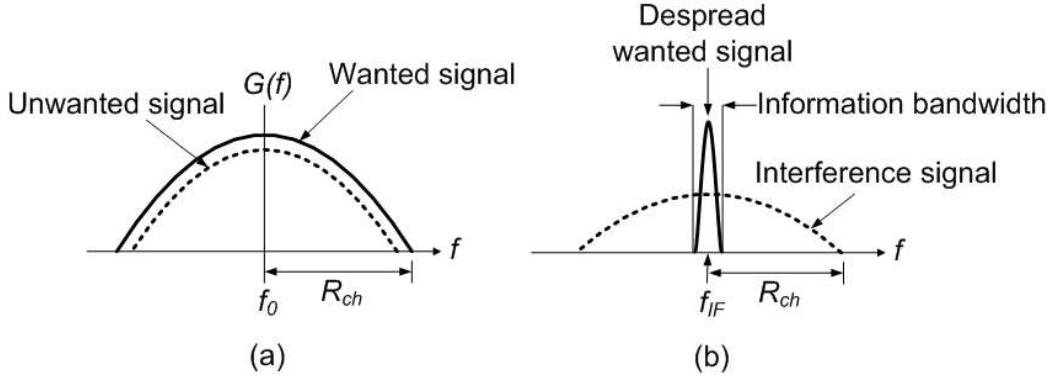
Figure 2.2: CDMA signal detection. (a) Wideband spectrum into the receiver consists of wanted and unwanted signals that are each spread by their unique code with code rate, R_{ch}. (b) Narrowband spectrum in the receiver after correlation with the user's unique code occupies a bandwidth centered at an intermediate frequency (IF), which is then applied to a demodulator.

frequency allocation, respectively. CDMA's RF spectrum at the input to the receiver and the RF spectrum after correlation with the correct synchronized pseudorandom number (PN) code is shown in Fig. 2.2.

2.2.1 Direct Sequence Code Division Multiple Access. A typical direct sequence-CDMA (DS-CDMA) system is shown in Fig. 2.3, where J is the total number of users. Fig. 2.3 shows user 1's data modulated, $u_1(t)$, then multiplied with a unique spreading signal, $h_1(t)$. Users 2 through J may also simultaneously spread their modulated data with spreading codes unique to them. As shown in Fig. 2.2, multiplication in the time-domain, $u(t)h(t)$, results in convolution in the frequency-domain [18], therefore, assuming $u(t)$ relatively occupies a narrow portion of the frequency spectrum compared with $h(t)$, the product signal, $u(t)h(t)$, will be approximately the bandwidth of $h(t)$.

In the absence of noise, the signal present at the receiver, $y(t)$, is defined as

$$y(t) = \sum_{n=1}^{J} u_n(t)h_n(t). \tag{2.1}$$

6

$$\int_0^T h_i(t)\, h_j(t)\, dt = \begin{cases} 1 \text{ for } i = j \\ 0 \text{ for } i \neq j \end{cases}$$
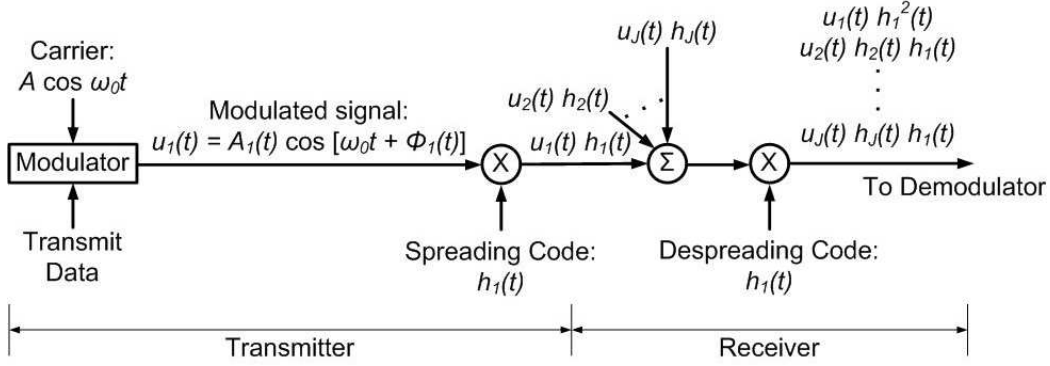
Figure 2.3: A direct sequence code division multiple access (DS-CDMA) system. Shown for spreading/despreading user 1's transmission.

The first stage of the receiver in Fig. 2.3 multiplies the incoming signal, (2.1), with a unique despreading code, $h_1(t)$, for example, to obtain the desired signal,

$$u_1(t)h_1^2(t), \tag{2.2}$$

plus unwanted signals,

$$u_2(t)h_2(t)h_1(t) + u_3(t)h_3(t)h_1(t) + \cdots + u_J(t)h_J(t)h_1(t). \tag{2.3}$$

If the spreading/despreading codes are chosen with orthogonal properties, as described in section 2.2.2, the desired signals can be extracted perfectly in the absence of noise. This is because $\int_0^T h_i^2(t)dt = 1$ and $\int_0^T h_i(t)h_j(t)dt = 0$ for $i \neq j$ [14].

The frequency-domain view of the DS-CDMA receiver is shown in Fig. 2.2. Fig. 2.2(a) depicts the wideband input into the receiver that consists of wanted and unwanted signals that are each spread by their own code with code rate, R_{ch}. Fig. 2.2(b) illustrates the RF spectrum after correlation with the user's unique code. The desired signal in (2.2) is centered at an intermediate frequency (IF) and occupies the information bandwidth. Typically the signal produced by (2.2) is then applied to

7

a demodulator with its bandwidth equal to the information bandwidth to pass the desired despread signal. The undesired signals of (2.3) remain spread by $h_1(t)h_n(t)$ and only the portion of the spectrum of the unwanted signals falling in the information bandwidth of the receiver will cause interference with the desired signal in the demodulation process [14].

2.2.2   Orthogonal Signals.   An example of orthogonal signals is shown in Fig. 2.4, where $u_1(t)$ and $u_2(t)$ are constructed from pulse waveforms described by $u_1(t) = p(t), 0 \leq t \leq T$ and $u_2(t) = p(t - \frac{T}{2}), 0 \leq t \leq T$, T is the symbol period, and $p(t)$ is a pulse with duration $\tau = \frac{T}{2}$. As described in [14, 18], a set of equal energy signals $u_i(t)$, where $i = 1, 2, \ldots, J$, is orthogonal if and only if

$$c_{ij} = \frac{1}{E} \int_0^T u_i(t)u_j(t)dt = \begin{cases} 1, & i = j \\ 0, & i \neq j \end{cases}, \tag{2.4}$$

where c_{ij} is the cross-correlation coefficient, and E is the signal energy, defined as

$$E = \int_0^T u_i^2(t)dt. \tag{2.5}$$

An example of computing the cross-correlation between two orthogonal signals at the waveform level is illustrated in Fig. 2.5(a).

2.2.3   Waveform Coding.   The ultimate goal of waveform coding is to produce the smallest cross-correlation result from (2.4) among all pairs of signals. According to [14, 18, 23], it is possible to make the cross-correlation coefficient equal to zero.

(2.4) presents a definition of orthogonality in terms of waveforms $u_i(t)$ and $u_j(t)$, where $i, j = 1, \ldots, M$, and M is the size of the waveform set. Each waveform in the set $\{u_i(t)\}$ consists of a sequence of pulses, where each pulse is designated with a level +1 or -1, which in turn represents the binary digit 1 or 0, respectively. When the set is expressed in binary, (2.4) becomes

8

| Analytic Representation | Waveform Representation | Vector Representation |

$u_1(t)$

$u_1(t) = p(t)$

$u_2(t) = p(t - \frac{T}{2})$

$0 \le t \le T$

$u_2(t)$
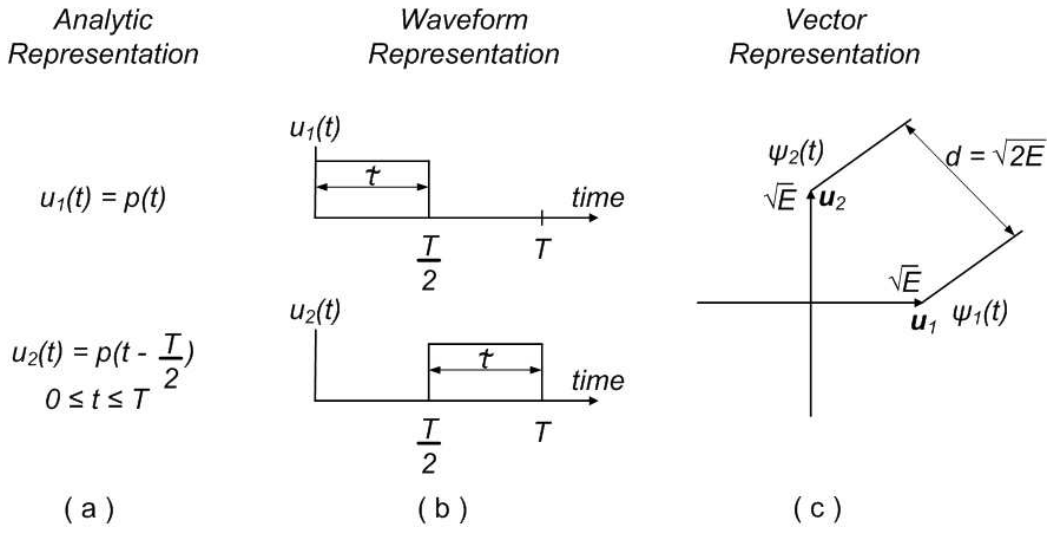
Figure 2.4: Binary Orthogonal Signals. (a) Analytic representation of orthogonal signals, $u_1(t)$ and $u_2(t)$. (b) $u_1(t)$ and $u_2(t)$ cannot interfere with one another because they are disjoint in time. (c) Vector representation illustrating the perpendicular relationship between signals $u_1(t)$ and $u_2(t)$.

$$c_{ij} = \frac{\sharp \text{ digit agreements} - \sharp \text{ digit disagreements}}{\sharp \text{ total digits in sequence}} = \begin{cases} 1, & i = j \\ 0, & i \neq j \end{cases}. \qquad (2.6)$$

An example of computing the cross-correlation between two orthogonal signals at the bit level is illustrated in Fig. 2.5(b).

2.2.4 Orthogonal Codes. As described in [14], orthogonal codewords of two digits each can be used to transform a one-bit data set, $\mathbf{B}_1$, described by the rows of the matrix $\mathbf{H}_1$ as

$$\mathbf{B}_1 = \begin{bmatrix} 0 \\ 1 \end{bmatrix}, \quad \mathbf{H}_1 = \begin{bmatrix} 0 & 0 \\ 0 & 1 \end{bmatrix}. \qquad (2.7)$$

(2.6) can be used to verify the orthogonality of the codeword set, $\mathbf{H}_1$. To encode a 2-bit data set, $\mathbf{B}_2$, $\mathbf{H}_2$ will be defined as

9

$$v_1 = [0\ 0\ 1\ 1]$$
$$v_2 = [0\ 1\ 1\ 0]$$

$$c_{ij} \equiv \frac{1}{\sqrt{E_{ci} \cdot E_{cj}}} \int_0^{T_s} \{\, c_i(t) \cdot c_j(t)\,\}\, dt$$

$$c_{12} \equiv \frac{1}{\sqrt{E_{c1} \cdot E_{c2}}} \int_0^{T_s} \left\{ \ldots \right\} dt$$

$$c_{12} \equiv \frac{1}{\sqrt{E_{c1} \cdot E_{c2}}} \cdot \{\, B_1\, B_2\, (+T_c - T_c + T_c - T_c)\,\}$$

$$c_{12} \equiv \frac{B_1 \cdot B_2 \cdot (0)}{\sqrt{B_1^2 T_s \cdot B_2^2 T_s}} = 0$$

$$c_{ij} \equiv \frac{\#\ Agree\ -\ \#\ Disagree}{Total}$$

$$c_{12} \equiv \frac{2-2}{4} = 0$$

(a)   (b)
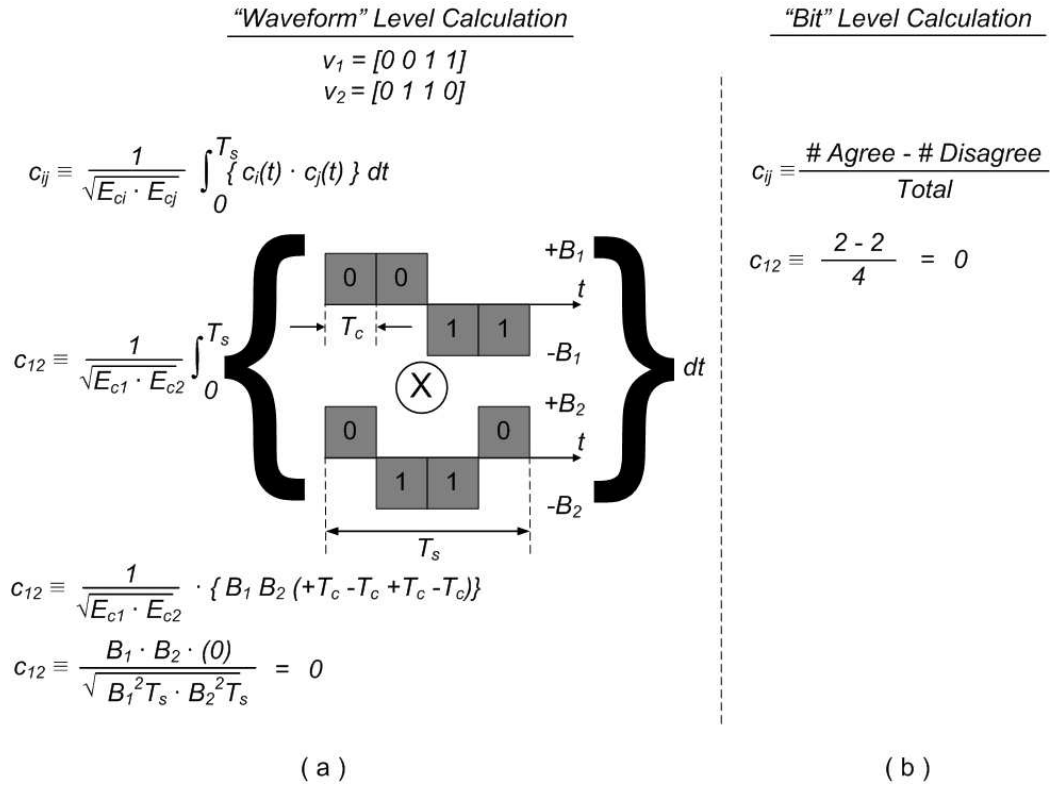
Figure 2.5: Cross-Correlation Between Orthogonal Signals. (a) Waveform level calculation of the cross-correlation between two orthogonal signals. (b) Bit level calculation of the cross-correlation between two orthogonal signals.

$$\mathbf{B}_2 = \begin{bmatrix} 0 & 0 \\ 0 & 1 \\ 1 & 0 \\ 1 & 1 \end{bmatrix}, \qquad \mathbf{H}_2 = \left[\begin{array}{cc|cc} 0 & 0 & 0 & 0 \\ 0 & 1 & 0 & 1 \\ \hline 0 & 0 & 1 & 1 \\ 0 & 1 & 1 & 0 \end{array} \right] = \begin{bmatrix} \mathbf{H}_1 & \mathbf{H}_1 \\ \mathbf{H}_1 & \overline{\mathbf{H}_1} \end{bmatrix}. \qquad (2.8)$$

$\mathbf{H}_2$'s lower right quadrant is the complement of the prior codeword set. Continuing the construction rule to obtain an orthogonal set $\mathbf{H}_3$ for a 3-bit data set, $\mathbf{B}_3$, produces

$$\mathbf{B}_3 = \begin{bmatrix} 0 & 0 & 0 \\ 0 & 0 & 1 \\ 0 & 1 & 0 \\ 0 & 1 & 1 \\ 1 & 0 & 0 \\ 1 & 0 & 1 \\ 1 & 1 & 0 \\ 1 & 1 & 1 \end{bmatrix}, \quad \mathbf{H}_3 = \left[\begin{array}{cccc|cccc} 0 & 0 & 0 & 0 & 0 & 0 & 0 & 0 \\ 0 & 1 & 0 & 1 & 0 & 1 & 0 & 1 \\ 0 & 0 & 1 & 1 & 0 & 0 & 1 & 1 \\ 0 & 1 & 1 & 0 & 0 & 1 & 1 & 0 \\ \hline 0 & 0 & 0 & 0 & 1 & 1 & 1 & 1 \\ 0 & 1 & 0 & 1 & 1 & 0 & 1 & 0 \\ 0 & 0 & 1 & 1 & 1 & 1 & 0 & 0 \\ 0 & 1 & 1 & 0 & 1 & 0 & 0 & 1 \end{array} \right] = \begin{bmatrix} \mathbf{H}_2 & \mathbf{H}_2 \\ \mathbf{H}_2 & \overline{\mathbf{H}}_2 \end{bmatrix}. \quad (2.9)$$

In general, construction of a codeword set, $\mathbf{H}_n$, of dimension $2^n \times 2^n$, is called a Hadamard matrix. For a n-bit data set, $\mathbf{H}_n$ is defined as

$$\mathbf{H}_n = \begin{bmatrix} \mathbf{H}_{n-1} & \mathbf{H}_{n-1} \\ \mathbf{H}_{n-1} & \overline{\mathbf{H}}_{n-1} \end{bmatrix}. \quad (2.10)$$

Each pair of words in each codeword set $\mathbf{H}_1$, $\mathbf{H}_2$, ..., $\mathbf{H}_n$ has equal number of digit agreements and digit disagreements [7], and, as defined in (2.6), $c_{ij} = 0$ for $i \neq j$, which makes each of the codeword sets orthogonal.

2.3   Quadrature Phase Shift Keying

Consider an original data stream, $d_0, d_1, d_2, \ldots$ consisting of bipolar pulses shown in Fig. 2.6(a); that is, the values of $d(t)$ are $+1$ and -1, representing binary one and zero, respectively. $d(t)$ can be divided into an in-phase stream, $d_I(t)$, and a quadrature stream, $d_Q(t)$, illustrated in Fig. 2.6(b), as

11
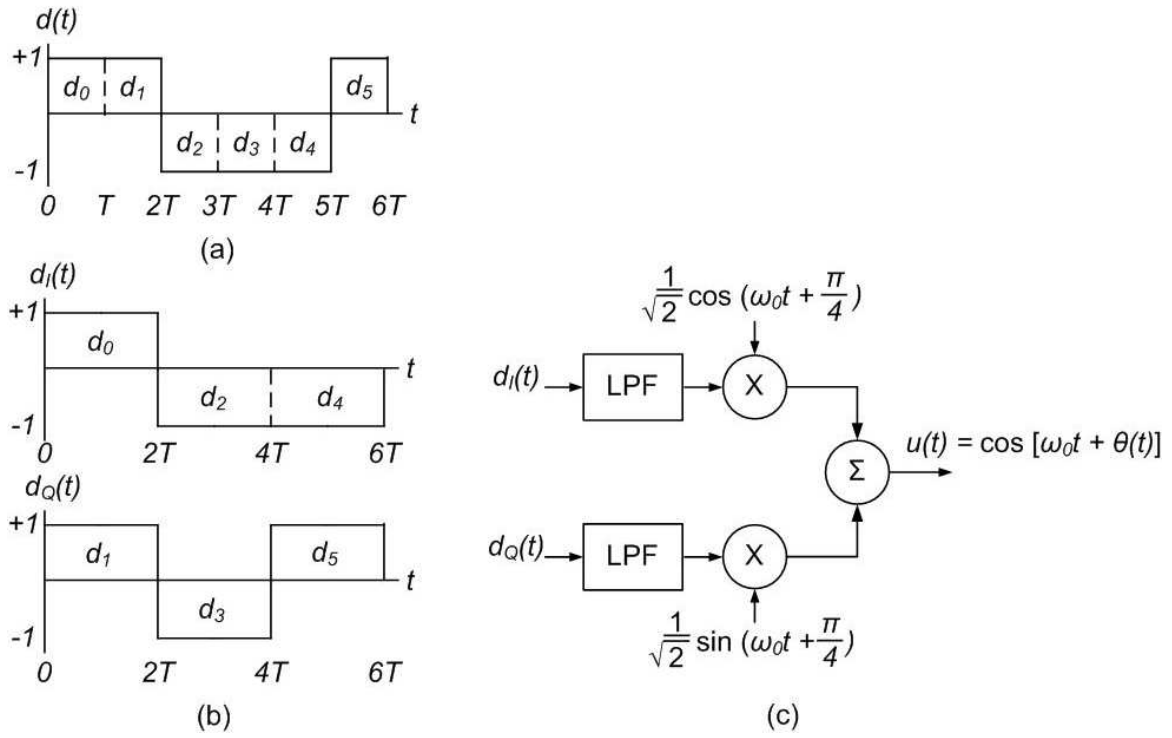
Figure 2.6: Illustrations of BPSK. (a) BPSK original data stream consisting of bipolar pulses. (b) Pulse stream divided into an in-phase stream, $d_I(t)$, and a quadrature stream, $d_Q(t)$. (c) A BPSK modulator.

$$d_I(t) = d_0, d_2, d_4, \ldots$$

(2.11)

$$d_Q(t) = d_1, d_3, d_5, \ldots,$$

where $d_I(t)$ is the even bits and $d_Q(t)$ is the odd bits of the original data stream, $d(t)$.

A convenient orthogonal realization of a QPSK waveform, $u(t)$, is achieved by amplitude modulating the in-phase and quadrature data streams onto the cosine and sine functions of a carrier wave, as defined in [14] as

$$u(t) = \frac{1}{\sqrt{2}} d_I(t) \cos\left(\omega_0 t + \frac{\pi}{4}\right) + \frac{1}{\sqrt{2}} d_Q(t) \sin\left(\omega_0 t + \frac{\pi}{4}\right). \qquad (2.12)$$

12
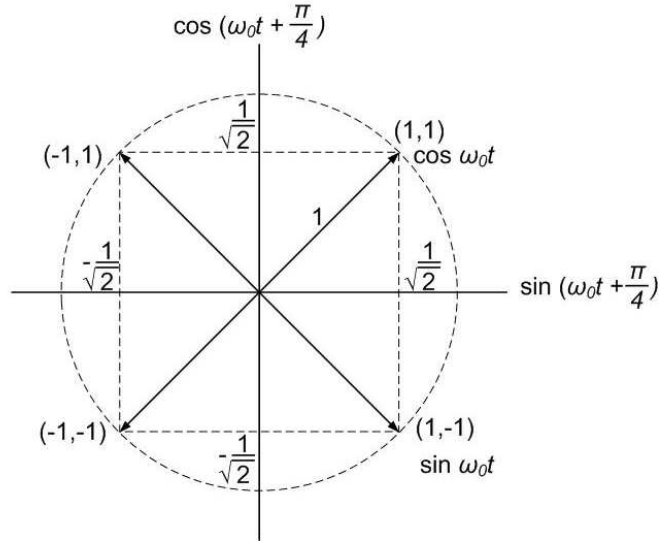
Figure 2.7: QPSK and OQPSK Signal Space. Due to the fact that $\cos\left(\omega_0 t + \frac{\pi}{4}\right)$ and $\sin\left(\omega_0 t + \frac{\pi}{4}\right)$ are orthogonal, the two BPSK signals can be detected separately.

Using trigonometric identities in $[13, 15]$, (2.12) can be written as

$$u(t) = \cos\left[\omega_0 t + \theta(t)\right], \tag{2.13}$$

which is shown in in Fig. 2.6(c).

The pulse stream, $d_I(t)$, amplitude-modulates the cosine function with an amplitude of ± 1, which is equivalent to a binary phase shift keying (BPSK) waveform because the phase of the cosine function is shifted by either 0 or π. Similarly, the pulse stream, $d_Q(t)$, modulates the sine function to produce a BPSK waveform that is orthogonal to the cosine function. The summation of these two orthogonal components of the carrier yeilds the QPSK waveform. The value of $\theta(t)$ will correspond to one of the four possible combinations of $d_I(t)$ and $d_Q(t)$ in (2.12): $\theta(t) = 0, \pm\frac{\pi}{2}$, or π. The signal vectors are shown in Fig 2.7.

13
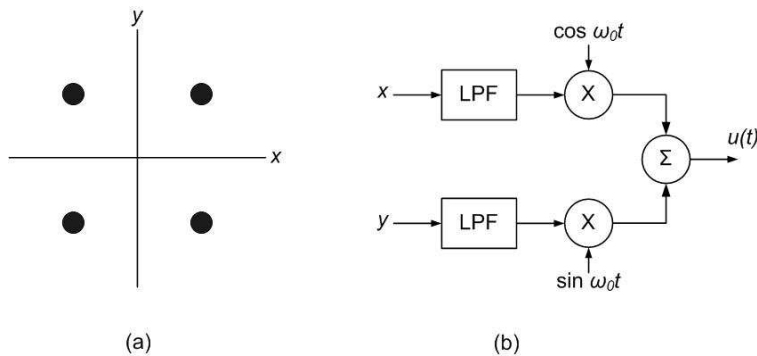
Figure 2.8: Illustrations of QAM. (a) 4-ary signal space. Oftentimes for convenience, 4-QAM data is represented by $\pm 1 \pm j$. (b) A general QAM modulator.

2.4 Quadrature Amplitude Modulation

QAM consists of two independently amplitude-modulated carriers in quadrature, which is considered a logical extension of QPSK [14]. Each block of m bits (m assumed even) can be split into two ($\frac{m}{2}$)-bit blocks which use ($\frac{m}{2}$)-bit digital-to-analog converters to provide the required modulating voltages for the carriers. At the receiver, each of the two signals is independently detected using matched filters [14]. Fig. 2.8(a) illustrates a two-dimensional signal space and a set of 4-ary QAM signal vectors or points arranged in a rectangular constellation. Oftentimes, 4-QAM data is conveniently represented as $\pm 1 \pm j$. A general QAM modulator is shown in Fig. 2.8(b).

2.5 Transform Domain Communication System

TDCS is a communications system that is designed for covert operations because of the security provided to its users by its inherent low probability of detection (LPD) and low probability of intercept (LPI) [2,3]. TDCS is a LPI/LPD communications system because of its ability to utilize a noise-like time-domain communications waveform while simultaneously avoiding interfering signals in the RF spectrum of interest.
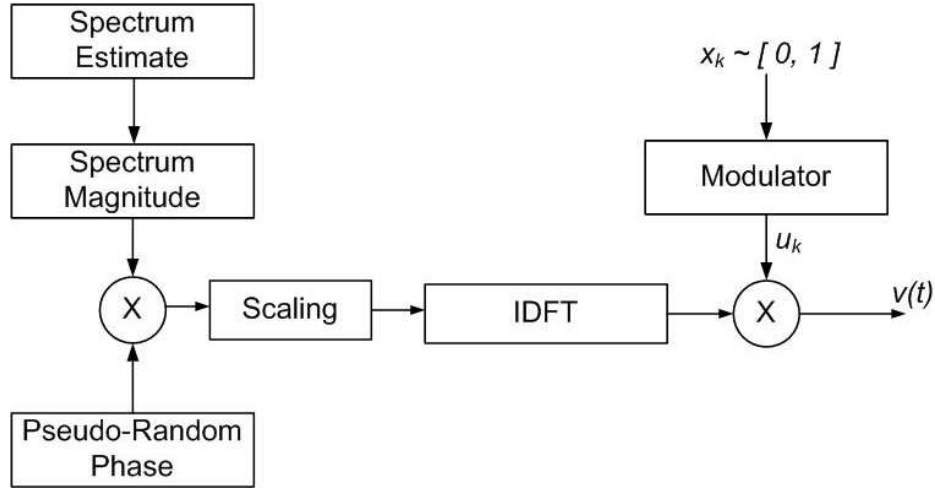
Figure 2.9:   Typical configuration of a TDCS transmitter.

2.5.1 TDCS Transmitter.   A typical TDCS transmitter is illustrated in Fig. 2.9 [3], where x_k represents a TDCS user's binary data to transmit, u_k denotes a TDCS user's modulated data symbol, and $v(t)$ represents the TDCS transmission signal.

2.5.1.1 Spectrum Estimate.   There are several methods of obtaining information on the frequency spectrum available for the TDCS transmissions [2,6,12, 16], but basically the regions of the frequency spectrum containing interference are identified to be avoided.

2.5.1.2 Spectrum Magnitude.   The purpose of the spectrum magnitude is to construct a frequency-domain communications waveform, referred to by Chakravarthy *et al.* as the fundamental modulation waveform (FMW) [2]. This identifies regions of the frequency spectrum to avoid based on a the spectrum estimate, which yields a communications waveform whose power spectral density (PSD) contains zero power in the portion of the spectrum identified as having interference present. This produces a vector of magnitude components, $A'(\omega)$, valued at either 1 or 0, whose values correspond to interference at given frequencies ω based on the spectrum estimate that are below or above, respectively, a specific LPD/LPI thresh-
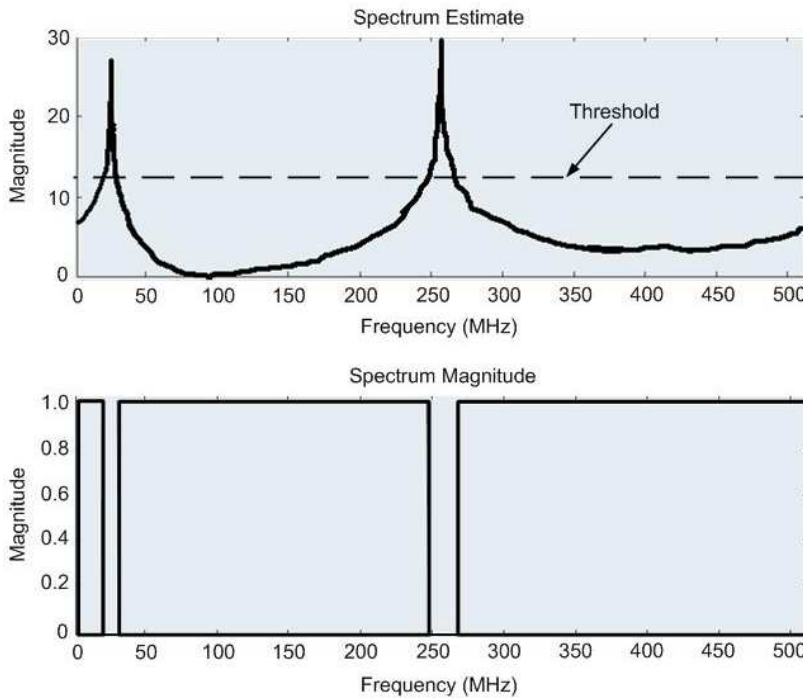
Figure 2.10:   An example of TDCS' functionality of the spec-
trum estimate and spectrum magnitude.

old [3]. The spectrum estimate and spectrum magnitude are illustrated in Fig. 2.10.
Note that this creates a FMW with the null-tones required by the DMT-FEQ.

2.5.1.3   Pseudo-Random Phase.   This provides the covert applicability
to TDCS via a complex pseudorandom phase vector because this produces a noise-
like time-domain communications waveform [2]. As described in [9], TDCS multiple
access networks can then be constructed by using the pseudorandom phase vector as a
spreading code. The pseudorandom phase vector must be generated on a symbol-by-
symbol basis in order to ensure TDCS transmissions maintain a noise-like appearance
over time, which secures TDCS' LPI/LPD status.

2.5.1.4   Scaling.   Scaling ensures an appropriate amount of energy is
contained in the communications symbol to be transmitted, and that all communica-
tions symbols contain uniform energy [2]. The uniform energy throughout a TDCS
waveform is important because of the noise-like structure of a TDCS waveform.

16
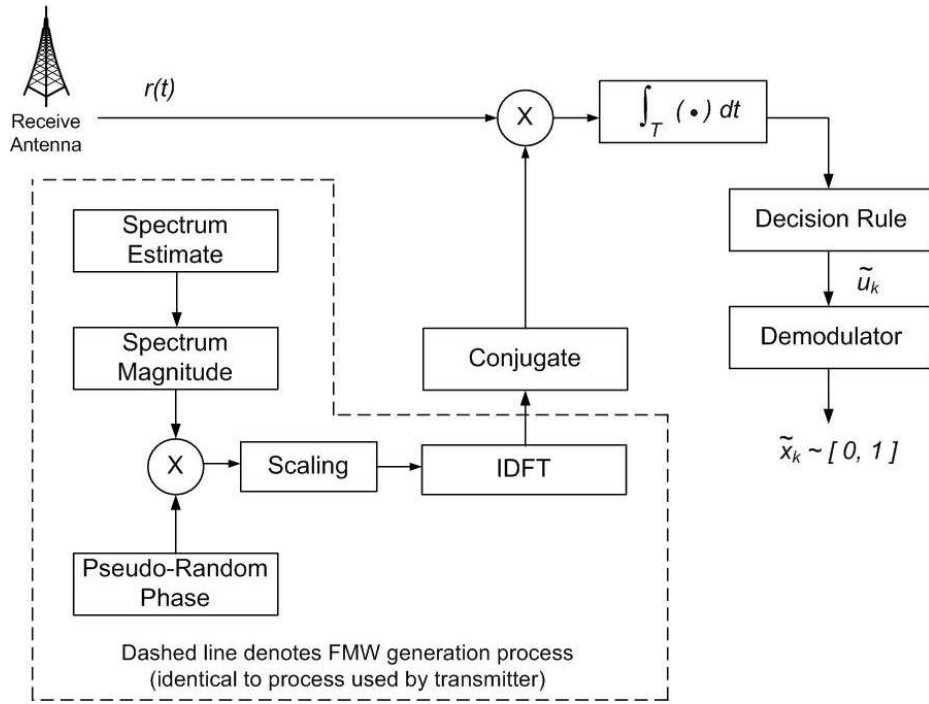
Figure 2.11:   Typical configuration of a TDCS receiver. Note
that the devices enclosed by the dashed line perform FMW gen-
eration identical to the process used by the TDCS transmitter.

2.5.1.5   IDFT and Modulator.   The purpose of the inverse discrete
Fourier transform (IDFT) and modulator are self-explanitory, and it is assumed the
reader need no further explanations on these functions.

2.5.2   TDCS Receiver.   A typical TDCS receiver is illustrated in Fig. 2.11 [3],
where $\tilde{u}_k$ denotes the estimate of a TDCS user's modulated data symbol and $\tilde{x}_k$
represents the estimate of a TDCS user's binary data that was received.

III. Discrete-Multitone Frequency-Domain Equalization Implementation

This chapter describes the implementation of the discrete-multitone (DMT) frequency-domain equalizer (FEQ) described in [20–22] in conjunction with two different types of communications systems that inherently possess null-tones in their respective transmission carrier frequencies. The first system is a code-division multiple access (CDMA) system utilizing Hadamard spreading codes for one to 32 synchronous users and the second system is a transform-domain communications system (TDCS) for one user.

The Hadamard encoded system is illustrated in Fig. 3.1 and consists of system users' binary data, 4-QAM modulator, channel, DMT-FEQ, post-equalized null-tone insertion, maximum likelihood estimation (MLE), decision function, and a 4-QAM demodulator. Note that the MLE has three possible estimators: 1) a scalar MLE (described in section 3.1.4) which requires, 2) an initial scalar approximate MLE (described in section 3.1.4.4), or 3) a vector MLE (described in section 3.1.5).

The TDCS implementation is illustrated in Fig. 3.14 and consists of a transmitter (described in section 2.5.1), DMT-FEQ, and a receiver (described in section 2.5.2).

3.1 Hadamard Encoded CDMA System with DMT-FEQ

The DMT-FEQ described in [20–22] completely eliminates interchannel interference (ICI) and intersymbol interference (ISI) when N carrier frequencies are used and K unused carrier frequencies (or null tones) are present. The total number of carrier frequencies is M and is defined as $M = N + K$. Note that certain conditions must be met in order for the DMT-FEQ to mitigate ICI and ISI, which are discussed in section 3.1.1.

The spreading codes used to distinguish individual users are assumed to be synchronous and can therefore be modeled as an orthogonal Hadamard matrix [8]. As shown in Fig. 3.2, Hadamard codes inherently possess null-tones in the frequency

18
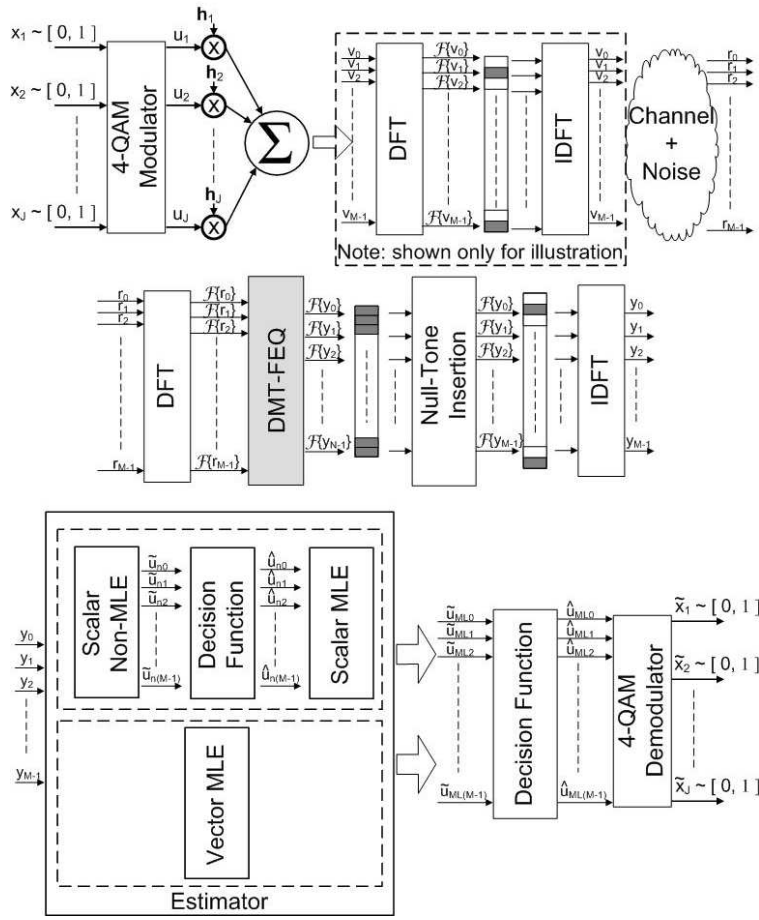
Figure 3.1:   A complete view of the Hadamard encoded CDMA
communications system. Note that when the post-equalized re-
ceived signal, $\mathbf{y}$, enters the estimator, it is either routed through
the scalar estimator or the vector estimator. Whichever estima-
tor the equalized signal is routed through, the output is $\tilde{\mathbf{u}}_{ML}$.

domain which make them an ideal candidate as a method to: 1) distinguish data

between users in a multi-user system and 2) keep null-tones intact in order to ex-

ploit properties of the DMT-FEQ to mitigate ISI and ICI from a non-ideal channel

corrupted by noise. More discussion of correctly chosen combinations of Hadamard

codes will be available in section 3.1.1.
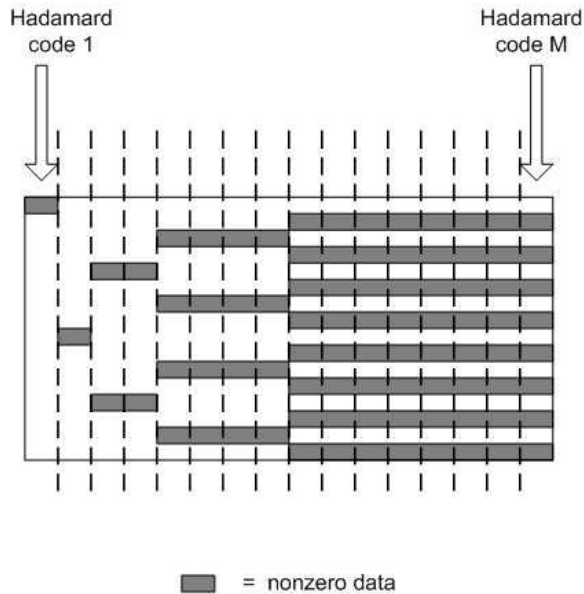
Figure 3.2: A view of Hadamard codes in the frequency domain show their inherent null tones. Shown for $M = 16$.

3.1.1 Transmitter. The time-domain transmission signal, denoted by the vector, $\mathbf{v}$, is the Hadamard encoded multi-user 4-QAM vector prior to transmission and is defined as

$$\mathbf{v} = \sum_{n=1}^{J} u_n \mathbf{h}_n, \tag{3.1}$$

where J is the total number of users in the system, u_n is the n-th user's 4-QAM symbol, and $\mathbf{h}_n$ is n-th user's Hadamard codeword. (3.1) is similar to (2.1) in all respects, except (3.1) uses vector notation.

It is important to correctly create $\mathbf{v}$ so that the DMT-FEQ will be able to equalize the received signal properly. A correctly chosen combination of Hadamard codes is one where equation (3.1) keeps an appropriate number of null-tones intact in the frequency-domain of the transmission vector that does not violate either of the two-case null-tone rules noted in [20–22]: Case one is $K \geq L_c - 1, L_c - 1 < 2N$, Case two is $K \geq 2N, L_c - 1 \geq 2N$, and L_c is the length of the channel impulse response (CIR). In other words, case one states the number of null-tones must be

20
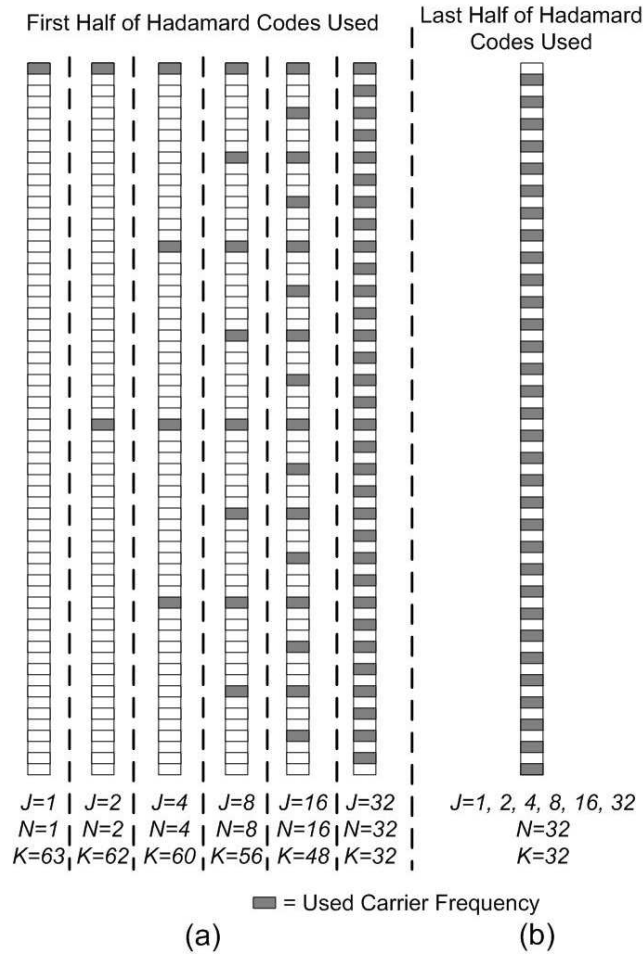
Figure 3.3: A frequency-domain view of users' null-tone impact in a Hadamard encoded CDMA communications system. Shown for $M = 64$. (a) Null-tones vary when spreading codes from the first half of a Hadamard matrix are used. (b) Null-tones remain uniform as long as the users, $J \leq 32$.

equal to, or greater than, the length of the CIR minus 1, and the length of the CIR minus one must be less than twice the number of used carrier frequencies. Case two states the number of null-tones must greater than, or equal to, twice the amount of used carrier frequencies and the CIR minus one must be greater than, or equal to, twice the amount of used carrier frequencies. Case two only applies when $N \leq \frac{M}{3}$, which is an impractical method of utilizing the allocated frequency spectrum of a communications system if only $\frac{1}{3}$ of the total carrier frequencies are utilized. Case two will only apply when spreading codes from the first half of the Hadamard matrix

$$\mathcal{F}\{\mathbf{v}\}=\sum_{n=1}^{J}u_n\cdot\mathcal{F}\{\mathbf{h_n}\}$$

Figure 3.4: A frequency-domain view of a transmission vector, $\mathcal{F}\{\mathbf{v}\}$, created by a correctly chosen combination of Hadamard codes for a CDMA communication system with $J = 8$ users, $L_c = 9$, $M = 16$ carrier frequencies, $N = 8$ used carrier frequencies, and $K = 8$ null-tones. This is a correct combination of Hadamard codes because it does not violate DMT-FEQ requirements $K \geq L_c - 1$ and $L_c - 1 < 2N$.

are used and the users, $J \leq 16$. Please refer to Fig. 3.3 for an illustration on the impact of the number of system users on the frequency-domain characteristics of a Hadamard encoded CDMA communications system's transmission signals.

Proceeding with a Hadamard encoded CDMA communications system that follows the case one rule set, two options exist for a transmission vector, $\mathbf{v}$, composed of correctly chosen combinations of Hadamard codes shown in Fig. 3.2, where $L_c = 9$ and $J = 8$ users. Note that the numbers provided are a simplified example for illustration purposes only. Since $M = 16$, one option is to use the first half of the Hadamard matrix ($\mathbf{h}_{1:8}$) which will make (3.1) become $\mathbf{v} = \sum_{n=1}^{J} u_n \mathbf{h}_n = u_1 \mathbf{h}_1 + u_2 \mathbf{h}_2 + \cdots + u_8 \mathbf{h}_8$, and the second option is to use $\mathbf{h}_{9:16}$ which will make (3.1) become $\mathbf{v} = \sum_{n=1}^{J} u_n \mathbf{h}_n = u_1 \mathbf{h}_9 + u_2 \mathbf{h}_{10} + \cdots + u_8 \mathbf{h}_{16}$. Both of these options do not violate case 1 because both instances of $\mathbf{v}$ contain eight null-tones, that is $K = 8$ in both examples given. Fig. 3.4

$$\mathcal{F}\{\mathbf{v}\}=\sum_{n=1}^{J}u_n\cdot\mathcal{F}\{\mathbf{h}_n\}$$
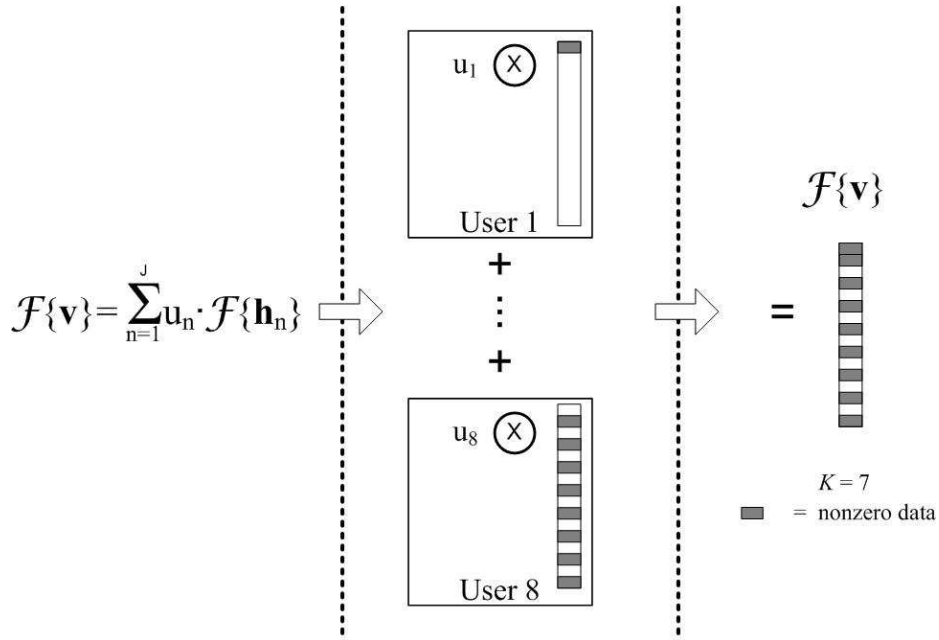
Figure 3.5: A frequency-domain view of a transmission vector, $\mathcal{F}\{\mathbf{v}\}$, created by an incorrectly chosen combination of Hadamard codes for a CDMA communication system w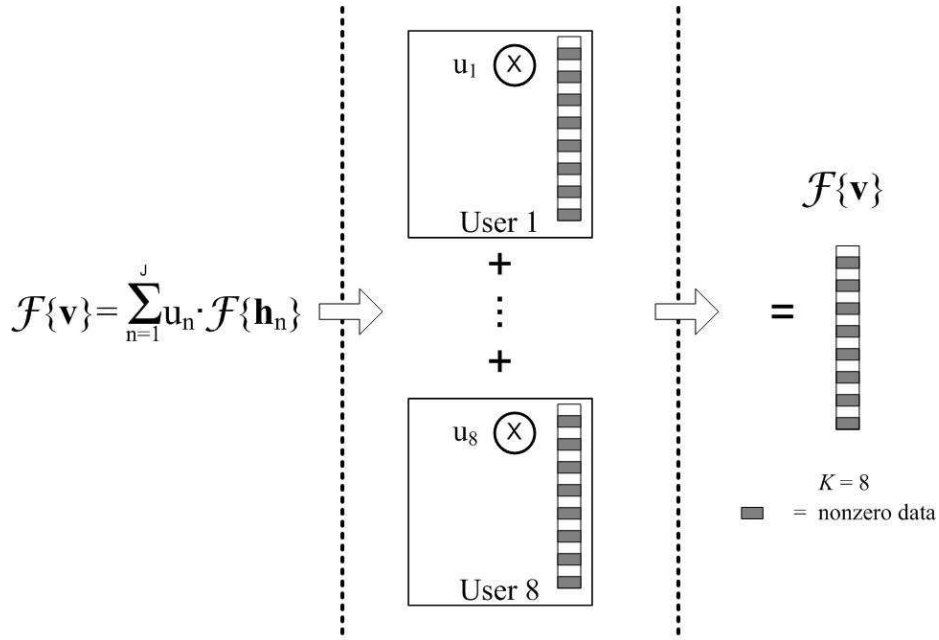ith $J = 8$ users, $L_c = 9$, $M = 16$ carrier frequencies, $N = 9$ used carrier frequencies, and $K = 7$ null-tones. This is an incorrect combination of Hadamard codes because it violates DMT-FEQ requirements $K \geq L_c - 1$ and $L_c - 1 < 2N$.

shows $\mathbf{v}$ constructed when Hadamard codes nine through sixteen are used from a 16×16 Hadamard matrix.

From the actual 64×64 Hadamard matrix used in the simulated system model, Fig. 3.3(a) and Fig. 3.3(b) depicts the following two scenarios that apply to the case one null-tone rule: 1) $J = 32$ users when the first half of the Hadamard codes are used and 2) $J \leq 32$ when the last half of the Hadamard codes are used. Fig. 3.3(a) illustrates when the case two null-tone rule applies: when the first half of the 64×64 Hadamard codes are used and when $J \leq 16$ users.

Many options exist for an incorrectly chosen combination of Hadamard codes shown in Fig. 3.2 with $L_c = 9$ and $J = 8$ users, but only one simplified example will be given. Since $M = 16$, one incorrect option is to use Hadamard code one and Hadamard codes nine through fifteen. This choice clearly violates case 1 because it
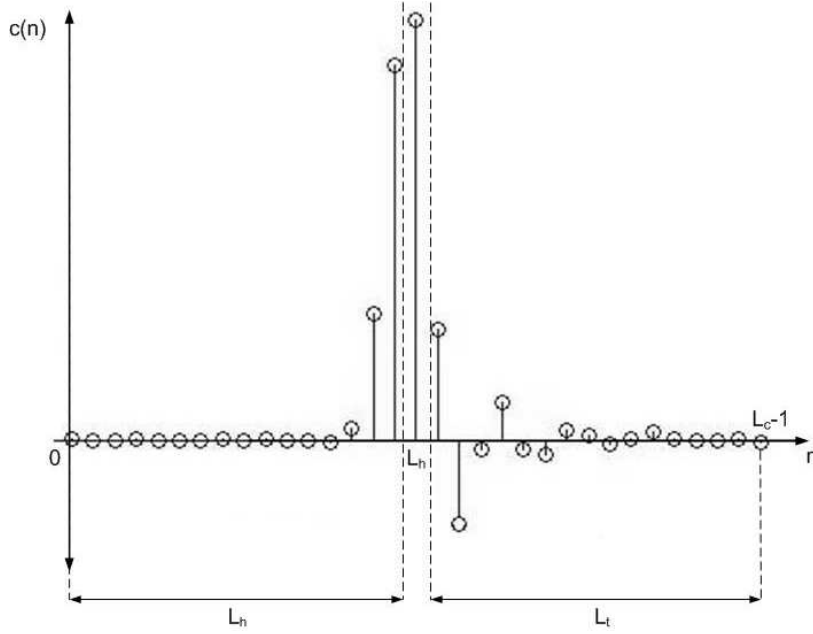
Figure 3.6:   A channel impulse response (CIR) is decomposed
into a head part, peak coefficient, and a tail part.

causes $K = 7$. Fig. 3.5 shows $\mathbf{v}$ constructed when using Hadamard code one and Hadamard codes nine through fifteen. Note that with J users, there are at most $M - J$ null tones, and fewer if the codewords are chosen incorrectly.

3.1.2   DMT-FEQ.   The receiver uses the CIR in the DMT-FEQ to identify and mitigate ICI and ISI by decomposing a channel matrix, $\mathbf{C}$, into a cyclic part and an error part, $\mathbf{C}_{\mathrm{cycl}}$ and $\mathbf{C}_{\mathrm{err}}$, respectively. $\mathbf{C}$ is defined as

$$\mathbf{C} = [\mathbf{C}_{\mathrm{t}}\ \mathbf{C}_{\mathrm{c}}\ \mathbf{C}_{\mathrm{h}}] = \mathbf{C}_{\mathrm{cycl}} + \mathbf{C}_{\mathrm{err}}, \tag{3.2}$$

where $\mathbf{C}_{\mathrm{t}}$, $\mathbf{C}_{\mathrm{c}}$, $\mathbf{C}_{\mathrm{h}}$, $\mathbf{C}_{\mathrm{cycl}}$, and $\mathbf{C}_{\mathrm{err}}$ are as defined in [20–22] based on the decomposition of the CIR into a head part, peak coefficient, and a tail part as shown in Fig. 3.6.

Decomposing $\mathbf{C}$ into $\mathbf{C}_{\mathrm{cycl}}$ and $\mathbf{C}_{\mathrm{err}}$ is due to the ICI and ISI producing properties of $\mathbf{C}$. ICI is produced when $\mathbf{C}_c$ does not possess a cyclic Toeplitz structure, ISI is produced from the preceeding symbol when $\mathbf{C}_t \neq 0$, and ISI is produced from the

24

following symbol when $\mathbf{C}_h \neq 0$. Therefore, $\mathbf{C}_{\text{err}}$ is the cause of ICI and ISI and is mitigated with the DMT-FEQ.

In a communications system with M total carrier frequencies, N used carrier frequencies, and K unused carrier frequencies, the DMT-FEQ uses selection matrices, $\mathbf{S}_0$ and $\mathbf{S}_1$, to eliminate nonrelevant rows and columns from the equalizer, $\mathbf{E}$. $\mathbf{S}_1$ is defined as

$$\mathbf{S}_1 = \text{diag}(s_0, s_1, \ldots, s_{M-1}), \tag{3.3}$$

with

$$s_i = \begin{cases} 1, & \text{if carrier is used} \\ 0, & \text{if carrier is not used} \end{cases}$$

and

$$\mathbf{S}_0 = \mathbf{I}_M - \mathbf{S}_1. \tag{3.4}$$

The selection matrices are then reduced to only non-zero columns, where $\mathbf{S}_0$ is reduced to a $M \times K$ matrix $\mathbf{S}_{0,\text{red}}$ and $\mathbf{S}_1$ is reduced to a $M \times N$ matrix $\mathbf{S}_{1,\text{red}}$. $\mathbf{D}$ is the diagonal matrix $\mathbf{D} = \text{diag}\left(d_0, d_1, \ldots, d_{M-1}\right)$, where $d_i = C\left(e^{\frac{j2\pi i}{M}}\right)$. Proceeding, $\mathbf{D}_{1,\text{red}} = \mathbf{S}_{1,\text{red}}^T \cdot \mathbf{D} \cdot \mathbf{S}_{1,\text{red}}$. Also, $\mathbf{W}_M$ and $\frac{\mathbf{W}_M^*}{M}$ denote the DFT and IDFT matrix, respectively, of size M. Another selection matrix, $\mathbf{Z}_{c,\text{red}}$, removes rows in $\mathbf{C}_{\text{err}}$ that do not contain relevant data and is used to define $\mathbf{W}_{0,\text{red}} = \mathbf{S}_{0,\text{red}}^T \cdot \mathbf{W}_M \cdot \mathbf{Z}_{c,\text{red}}^T$ and $\mathbf{W}_{1,\text{red}} = \mathbf{S}_{1,\text{red}}^T \cdot \mathbf{W}_M \cdot \mathbf{Z}_{c,\text{red}}^T$.

The reduction of $\mathbf{E}$ into $\mathbf{E}_{0,red}$ and $\mathbf{E}_{1,red}$ is shown in Fig. 3.7 and is performed in order to enhance the speed of the DMT-FEQ by eliminating non-relevant computations involving null-tones. Since equalization of a null-tone will effectively result in a null-tone, the DMT-FEQ disregards the null-tone information by using the reduced

25
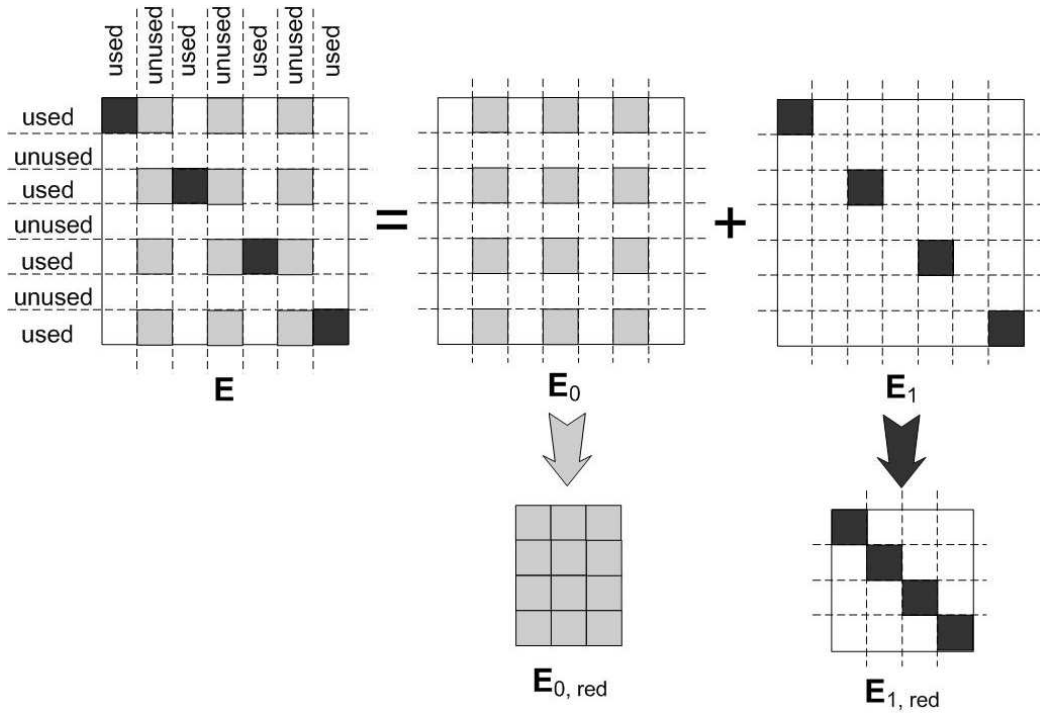
Figure 3.7: An equalizer is reduced to only relevant data. $\mathbf{E}_{0,red}$ contains null-tone data and $\mathbf{E}_{1,red}$ contains used carrier data.

forms of the equalizer, $\mathbf{E}_{0,red}$ and $\mathbf{E}_{1,red}$. As described in [20–22] and illustrated in Fig. 3.7, $\mathbf{E}_{0,red}$ and $\mathbf{E}_{1,red}$ are defined as

$$\mathbf{E}_{0,red} = -\mathbf{E}_{1,red} \cdot \mathbf{W}_{1,red} \cdot \mathbf{W}_{0,red}^{\dagger}, \tag{3.5}$$

and

$$\mathbf{E}_{1,red} = \mathbf{S}_{1,red} \cdot \mathbf{D}_{1,red}^{-1} \cdot \mathbf{S}_{1,red}^{T}, \tag{3.6}$$

where the pseudoinverse $\mathbf{W}_{0,red}^{\dagger}$ of $\mathbf{W}_{0,red}$ is defined as

$$\mathbf{W}_{0,red}^{\dagger} = \left(\mathbf{W}_{0,red}^{*}\mathbf{W}_{0,red}\right)^{-1}\mathbf{W}_{0,red}^{*} \tag{3.7}$$

and $\mathbf{W}_{0,red}^{*}$ denotes the complex conjugate of $\mathbf{W}_{0,red}$.
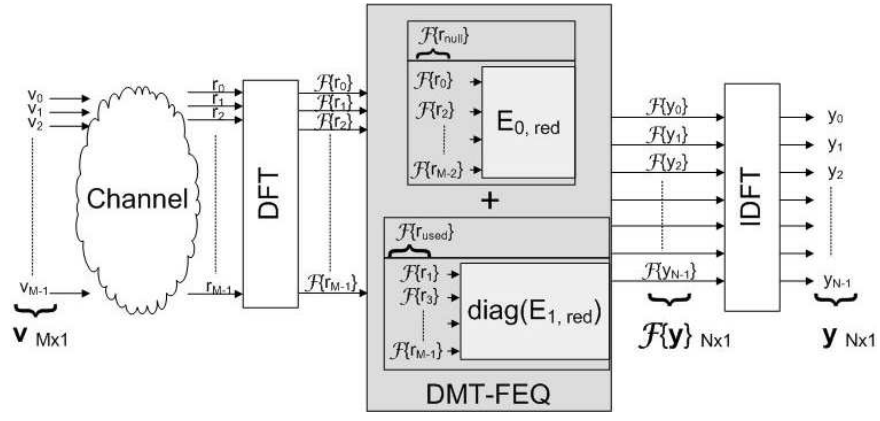
Figure 3.8:   The DMT-FEQ removes the K null-tones from the received signal. This causes $\mathcal{F}\{\mathbf{y}\}$ to be a vector with dimensions $N \times 1$, which will cause $\mathbf{y}$ to be an incorrect representation of the transmission vector, $\mathbf{v}$. The system shown above has null-tones occupying even numbered carrier frequencies.

3.1.3   Post-Equalization Null-Tone Insertion.   Due to the DMT-FEQ properties shown in Fig. 3.7 [20–22], a vector reduction occurs in the post-equalization $\mathcal{F}\{\mathbf{y}\}$, where the K null-tones once present in the frequency-domain transmission vector, $\mathcal{F}\{\mathbf{v}\}$, are removed from $\mathcal{F}\{\mathbf{y}\}$. The impact of the post-equalization null-tone removal in $\mathcal{F}\{\mathbf{y}\}$ will produce an inaccurate time-domain received signal, $\mathbf{y}$. This is illustrated in Fig. 3.8.

One solution that will correct the discrepancy between $\mathbf{v}$ and the post DMT-FEQ $\mathbf{y}$ is to insert null-tones into $\mathcal{F}\{\mathbf{y}\}$. Of course, the null-tone insertion needs to correspond to the null-tones that are present in $\mathcal{F}\{\mathbf{v}\}$. The null-tone insertion, or post-equalization expansion of the received signal, will increase $\mathcal{F}\{\mathbf{y}\}$ from an $N \times 1$ vector to a $M \times 1$ vector. This is shown in Fig. 3.9.

3.1.4   Scalar Maximum-Likelihood Estimation.   The maximum likelihood estimate (MLE) of a received symbol as described in [11] was used in order to determine the optimal estimate of a received symbol corrupted by noise.

27
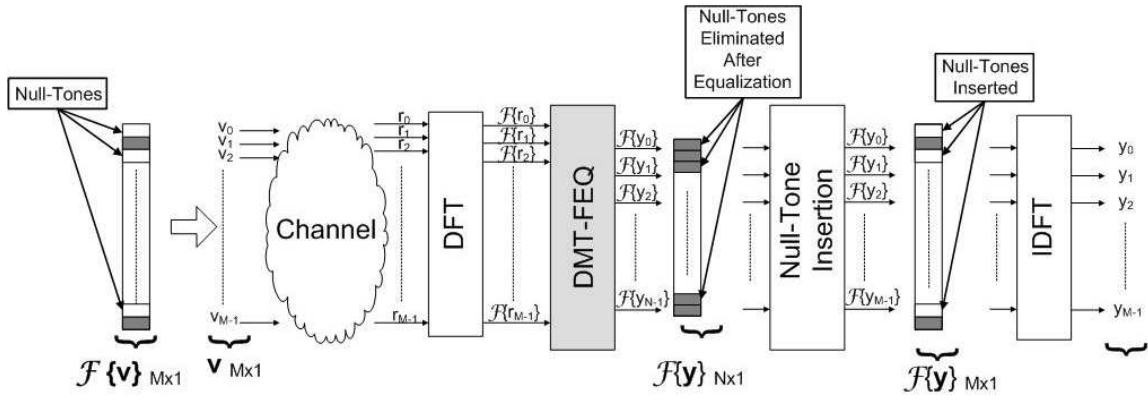
Figure 3.9:   Inserting null-tones in $\mathcal{F}\{\mathbf{y}\}$ corresponding to null-tones that occupy $\mathcal{F}\{\mathbf{v}\}$ creates an equalized signal, $\mathbf{y}$, that more accurately represents the transmission vector, $\mathbf{v}$.

Because the DMT-FEQ described in [20–22] completely eliminates ISI and ICI due to transmission through a non-ideal channel, the post-DMT-FEQ received symbol vector, $\mathbf{y}$, at the receiver becomes

$$\mathbf{y} = \mathbf{v} + \mathbf{n}, \tag{3.8}$$

where $\mathbf{v}$ is as defined in (3.1) and $\mathbf{n}$ is the processed additive noise (not necessarily white) plus residual ISI vector.

In a communication system with M carrier frequencies, $\mathbf{n}$ can be modeled as

$$\mathbf{n} \sim \mathcal{N}(\, \mathbf{0} \,,\, \mathbf{K} \,), \tag{3.9}$$

where

$$\mathbf{0} = \begin{bmatrix} 0_1 \\ 0_2 \\ \vdots \\ 0_M \end{bmatrix}$$

and

28

$$\mathbf{K} = \begin{bmatrix} \sigma_{11}^2 & \sigma_{12}^2 & \cdots & \sigma_{1M}^2 \\ \sigma_{21}^2 & \sigma_{22}^2 & \cdots & \sigma_{2M}^2 \\ \vdots & \vdots & \ddots & \vdots \\ \sigma_{M1}^2 & \sigma_{M2}^2 & \cdots & \sigma_{MM}^2 \end{bmatrix} = E[\mathbf{n}\,\mathbf{n}^H] \approx \frac{1}{P}\sum_{n=1}^{P} \mathbf{n}_n\,\mathbf{n}_n^H.$$

The noise covariance matrix, $\mathbf{K}$, can be obtained through a training period by solving for $\mathbf{n}$ in (3.8).

The distribution of $\mathbf{y}$ then becomes

$$\mathbf{y} \sim \mathcal{N}\left(\sum_{n=1}^{J} u_n \mathbf{h}_n ,\ \mathbf{K} \right). \tag{3.10}$$

The probability distribution function (PDF) of $\mathbf{y}$ given $\mathbf{v}$ then becomes

$$p(\mathbf{y}|\mathbf{v}) = \frac{1}{(2\pi)^J |\,\mathbf{K}|}\, e^{-(\mathbf{y}-\sum_{n=1}^{J} u_n \mathbf{h}_n)^H\ \mathbf{K}^{-1}\ (\mathbf{y}-\sum_{n=1}^{J} u_n \mathbf{h}_n)}. \tag{3.11}$$

The MLE of the transmitted symbol of interest as described in [11] is defined as

$$\tilde{u}_{k,ML}(\mathbf{y}|\mathbf{v}) = \arg\ \max_{u_k}\ p(\mathbf{y}|\mathbf{v}). \tag{3.12}$$

Since maximizing $p(\mathbf{y}|\mathbf{v})$ is equivalent to maximizing $\ln p(\mathbf{y}|\mathbf{v})$, equation (3.12) can be rewritten as

$$\tilde{u}_{k,ML}(\mathbf{y}|\mathbf{v}) = \arg\ \max_{u_k}\ \ln p(\mathbf{y}|\mathbf{v}). \tag{3.13}$$

(3.13) reduces to

$$\tilde{u}_{k,ML}(\mathbf{y}|\mathbf{v})$$

$$= \arg \max_{u_k} \ln \frac{1}{(2\pi)^J |\mathbf{K}|} - (\mathbf{y} - \sum_{n=1}^{J} u_n \mathbf{h}_n)^H \mathbf{K}^{-1} (\mathbf{y} - \sum_{n=1}^{J} u_n \mathbf{h}_n),$$

$$= \arg \max_{u_k} -(\mathbf{y} - \sum_{n=1}^{J} u_n \mathbf{h}_n)^H \mathbf{K}^{-1} (\mathbf{y} - \sum_{n=1}^{J} u_n \mathbf{h}_n),$$

$$= \arg \max_{u_k} -\mathbf{y}^H \mathbf{K}^{-1} \mathbf{y} + \mathbf{y}^H \mathbf{K}^{-1} \left(\sum_{n=1}^{J} u_n \mathbf{h}_n \right) + \left(\sum_{n=1}^{J} u_n \mathbf{h}_n \right)^H \mathbf{K}^{-1} \mathbf{y}$$

$$- \left(\sum_{n=1}^{J} u_n \mathbf{h}_n \right)^H \mathbf{K}^{-1} \left(\sum_{n=1}^{J} u_n \mathbf{h}_n \right),$$

$$= \arg \max_{u_k} -\mathbf{y}^H \mathbf{K}^{-1} \mathbf{y} + \mathbf{y}^H \mathbf{K}^{-1} \left(u_k \mathbf{h}_k + \sum_{n \neq k}^{J} u_n \mathbf{h}_n \right)$$

$$+ \left(u_k \mathbf{h}_k + \sum_{n \neq k}^{J} u_n \mathbf{h}_n \right)^H \mathbf{K}^{-1} \mathbf{y} - \left(u_k \mathbf{h}_k + \sum_{n \neq k}^{J} u_n \mathbf{h}_n \right)^H \mathbf{K}^{-1} \left(u_k \mathbf{h}_k + \sum_{n \neq k}^{J} u_n \mathbf{h}_n \right),$$

$$= \arg \max_{u_k} -\mathbf{y}^H \mathbf{K}^{-1} \mathbf{y} + \mathbf{y}^H \mathbf{K}^{-1} u_k \mathbf{h}_k + \mathbf{y}^H \mathbf{K}^{-1} \left(\sum_{n \neq k}^{J} u_n \mathbf{h}_n \right) + (u_k \mathbf{h}_k)^H \mathbf{K}^{-1} \mathbf{y}$$

$$+ \left(\sum_{n \neq k}^{J} u_n \mathbf{h}_n \right)^H \mathbf{K}^{-1} \mathbf{y} - (u_k \mathbf{h}_k)^H \mathbf{K}^{-1} (u_k \mathbf{h}_k) - (u_k \mathbf{h}_k)^H \mathbf{K}^{-1} \left(\sum_{n \neq k}^{J} u_n \mathbf{h}_n \right)$$

$$- \left(\sum_{n \neq k}^{J} u_n \mathbf{h}_n \right)^H \mathbf{K}^{-1} u_k \mathbf{h}_k - \left(\sum_{n \neq k}^{J} u_n \mathbf{h}_n \right)^H \mathbf{K}^{-1} \left(\sum_{n \neq k}^{J} u_n \mathbf{h}_n \right).$$

$$\text{(3.14)}$$

A necessary condition for the MLE is to set the derivative of (3.14) equal to zero, which becomes

$$\frac{d}{du_k} \ln p(\mathbf{y}|\mathbf{v}) \bigg|_{u_k = \tilde{u}_{k,ML}(\mathbf{y}|\mathbf{v})} = 0. \tag{3.15}$$

In order to clean up the derivation of $\tilde{u}_{k,ML}$ at the receiver we will proceed as follows: u_k is a scalar, therefore it is a term that can be factored out, and, since $\frac{d}{du_k}$

of non-u_k terms will inherently force them to zero, we will ignore them. Also, $\mathbf{h}_k$ is real, so $\mathbf{h}_k^* = \mathbf{h}_k$, where $\mathbf{h}_k^*$ denotes the complex conjugate of $\mathbf{h}_k$. Proceeding with these substitutions results in (3.15) becoming

$$\frac{d}{du_k}\left(\mathbf{y}^H\mathbf{K}^{-1}u_k\mathbf{h}_k + (u_k\mathbf{h}_k)^H\mathbf{K}^{-1}\mathbf{y} - (u_k\mathbf{h}_k)^H\mathbf{K}^{-1}(u_k\mathbf{h}_k)\right.$$
$$\left. - (u_k\mathbf{h}_k)^H\mathbf{K}^{-1}\left(\sum_{n\neq k}^J u_n\mathbf{h}_n\right) - \left(\sum_{n\neq k}^J u_n\mathbf{h}_n\right)^H\mathbf{K}^{-1}u_k\mathbf{h}_k\right) = 0$$

$$\frac{d}{du_k}\left(u_k\left(\mathbf{y}^H\mathbf{K}^{-1}\mathbf{h}_k\right) + u_k^*\left(\mathbf{h}_k^T\mathbf{K}^{-1}\mathbf{y}\right) - u_k^*u_k\left(\mathbf{h}_k^T\mathbf{K}^{-1}\mathbf{h}_k\right)\right.$$
$$\left. - u_k^*\left(\mathbf{h}_k^T\mathbf{K}^{-1}\left(\sum_{n\neq k}^J u_n\mathbf{h}_n\right)\right) - u_k\left(\left(\sum_{n\neq k}^J u_n\mathbf{h}_n\right)^H\mathbf{K}^{-1}\mathbf{h}_k\right)\right) = 0 \quad (3.16)$$

In order to reduce the clutter of (3.16), we will define $a_k = \mathbf{y}^H\mathbf{K}^{-1}\mathbf{h}_k$, $a_k^* = \mathbf{h}_k^T\mathbf{K}^{-1}\mathbf{y}$, $b_k = \mathbf{h}_k^T\mathbf{K}^{-1}\mathbf{h}_k$, $c_k = \mathbf{h}_k^T\mathbf{K}^{-1}\left(\sum_{n\neq k}^J u_n\mathbf{h}_n\right)$, and $c_k^* = \left(\sum_{n\neq k}^J u_n\mathbf{h}_n\right)^H\mathbf{K}^{-1}\mathbf{h}_k$. (3.16) becomes

$$\frac{d}{du_k}\left(u_k a_k + u_k^* a_k^* - u_k^* u_k b_k - u_k^* c_k - u_k c_k^*\right) = 0 \tag{3.17}$$

Since $u_k = (u_{k_{Re}} + j\, u_{k_{Im}})$, (3.16) becomes a derivative operation with respect to a complex parameter [4], which by definition is

$$\frac{d\, ln\, p(\mathbf{y}|\mathbf{v})}{du_k} = \frac{1}{2}\left(\frac{d\, ln\, p(\mathbf{y}|\mathbf{v})}{du_{k_{Re}}} - j\,\frac{d\, ln\, p(\mathbf{y}|\mathbf{v})}{du_{k_{Im}}}\right) = 0. \tag{3.18}$$

Solving (3.18)

31

$$\frac{1}{2}\frac{d}{du_{k_{Re}}}\Big((u_{k_{Re}}+ju_{k_{Im}})\,a_k+(u_{k_{Re}}-ju_{k_{Im}})\,a_k^*-(u_{k_{Re}}-ju_{k_{Im}})\,(u_{k_{Re}}+ju_{k_{Im}})\,b_k$$
$$-(u_{k_{Re}}-ju_{k_{Im}})\,c_k-(u_{k_{Re}}+ju_{k_{Im}})\,c_k^*\Big)-j\,\frac{1}{2}\frac{d}{du_{k_{Im}}}\Big((u_{k_{Re}}+ju_{k_{Im}})\,a_k$$
$$+(u_{k_{Re}}-ju_{k_{Im}})\,a_k^*-(u_{k_{Re}}-ju_{k_{Im}})\,(u_{k_{Re}}+ju_{k_{Im}})\,b_k-(u_{k_{Re}}-ju_{k_{Im}})\,c_k$$
$$-(u_{k_{Re}}+ju_{k_{Im}})\,c_k^*\Big)=0$$

$$\frac{1}{2}\frac{d}{du_{k_{Re}}}\Big(u_{k_{Re}}a_k+ju_{k_{Im}}a_k+u_{k_{Re}}a_k^*-ju_{k_{Im}}a_k^*-u_{k_{Re}}^2b_k-ju_{k_{Re}}u_{k_{Im}}b_k+ju_{k_{Re}}u_{k_{Im}}b_k$$
$$+j^2u_{k_{Im}}^2b_k-u_{k_{Re}}c_k+ju_{k_{Im}}c_k-u_{k_{Re}}c_k^*-ju_{k_{Im}}c_k^*\Big)$$
$$-j\,\frac{1}{2}\frac{d}{du_{k_{Im}}}\Big(u_{k_{Re}}a_k+ju_{k_{Im}}a_k+u_{k_{Re}}a_k^*-ju_{k_{Im}}a_k^*-u_{k_{Re}}^2b_k-ju_{k_{Re}}u_{k_{Im}}b_k$$
$$+ju_{k_{Re}}u_{k_{Im}}b_k+j^2u_{k_{Im}}^2b_k-u_{k_{Re}}c_k+ju_{k_{Im}}c_k-u_{k_{Re}}c_k^*-ju_{k_{Im}}c_k^*\Big)=0$$

$$\frac{1}{2}\left(a_k+a_k^*-2u_{k_{Re}}b_k-c_k-c_k^*\right)-\frac{1}{2}j\left(ja_k-ja_k^*-2u_{k_{Im}}b_k+jc_k-jc_k^*\right)=0$$

$$\frac{(a_k+a_k^*)}{2}-\frac{(c_k+c_k^*)}{2}-u_{k_{Re}}b_k-\frac{j^2a_k}{2}+\frac{j^2a_k^*}{2}+ju_{k_{Im}}b_k-\frac{j^2c_k}{2}+\frac{j^2c_k^*}{2}=0$$

$$(u_{k_{Re}}-ju_{k_{Im}})\,b_k=a_{k_{Re}}-c_{k_{Re}}+\frac{(a_k-a_k^*)}{2}+\frac{(c_k-c_k^*)}{2}$$

$$u_{k_{Re}}-ju_{k_{Im}}=\frac{(a_{k_{Re}}-c_{k_{Re}}+ja_{k_{Im}}+jc_{k_{Im}})}{b_k}$$

$$\tilde{u}_{k,ML}=\frac{(a_k-c_k)_{Re}-j\,(a_k+c_k)_{Im}}{b_k}$$

$$\tilde{u}_{k,ML}=\frac{(a_k^*-c_k)}{b_k}$$

$$\boxed{\tilde{u}_{k,ML}=\frac{\mathbf{h}_k^T\mathbf{K}^{-1}\left(\mathbf{y}-\sum_{n\neq k}^{J}u_n\mathbf{h}_n\right)}{\mathbf{h}_k^T\mathbf{K}^{-1}\mathbf{h}_k}}. \tag{3.19}$$

(3.19) states that $\tilde{u}_{k,ML}$ is the optimal scalar MLE of an individual user's modulated data. Note that $c_k=\mathbf{h}_k^T\mathbf{K}^{-1}\left(\sum_{n\neq k}^{J}u_n\mathbf{h}_n\right)$, which requires a-priori knowledge of all the other users' 4-QAM data and will be addressed in section 3.1.4.4.
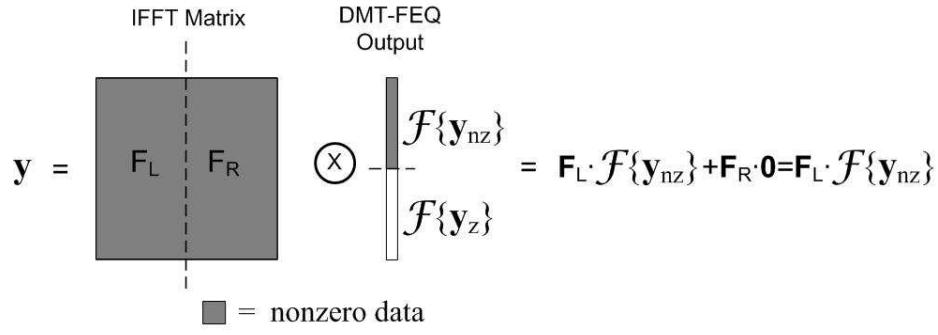
Figure 3.10: The output of the DMT-FEQ inherently contains null-tones, denoted as $\mathcal{F}\{\mathbf{y}_z\}$, which are passed on to the received signal vector, $\mathbf{y}$. The null-tones are shown grouped for simplicity.

3.1.4.1 Non-Invertible Noise Covariance Matrix. (3.19) requires the noise covariance matrix, $\mathbf{K}$, to be invertible, which is the case if $\mathbf{K}$ is of full rank, as described in [17]. This section describes the effects of null-tones on $\mathbf{K}$ and leads into section 3.1.4.2, which provides an alternative approach to obtain an invertible $\mathbf{K}$ when presented with a non-invertible $\mathbf{K}$, and will lead to obtaining $\tilde{u}_{k,ML}$.

Since the equalized signal, $\mathbf{y}$, and the transmission vector, $\mathbf{v}$, are known during a training period, the noise vector, $\mathbf{n}$, is obtained by solving (3.8). Fig. 3.10 is a simplified representation of null-tones in the output of the DMT-FEQ, where

$$\mathbf{y} = \mathbf{F}_L \cdot \mathcal{F}\{\mathbf{y}_{nz}\}. \tag{3.20}$$

In (3.20), $\mathbf{F}_L$ denotes the left portion of the IDFT matrix and $\mathcal{F}\{\mathbf{y}_{nz}\}$ denotes the frequency-domain non-zero data of the output of the DMT-FEQ. Solving (3.8) will lead to the fact that null-tones that are present in $\mathbf{y}$ will also be present in $\mathbf{n}$. Setting the signal component of $\mathbf{y}$ to zero and solving for $\mathbf{n}$ in (3.20) results in

$$\mathbf{n} = \mathbf{F}_L \cdot \mathcal{F}\{\mathbf{n}_{nz}\}. \tag{3.21}$$

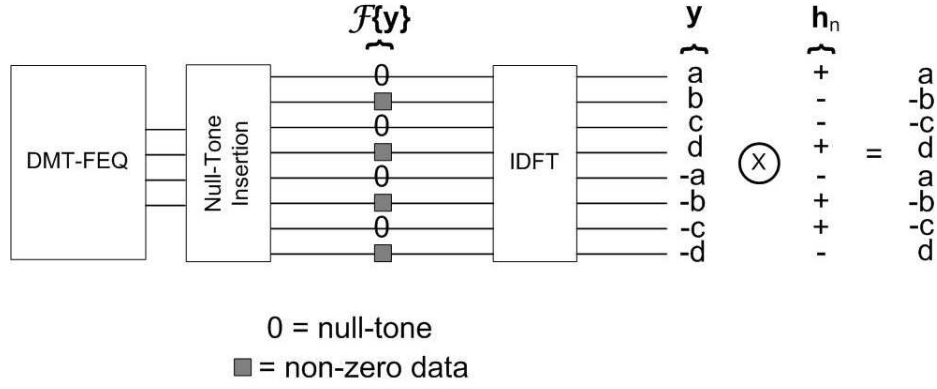Once $\mathbf{n}$ is obtained, $\mathbf{K}$ becomes

33

Figure 3.11: Null-tones affect the received signal vector $\mathbf{y}$ by causing linear dependence of its terms.

$$\mathbf{K} = E[\mathbf{n} \cdot \mathbf{n}^H] \;=\; E[\mathbf{F}_L \mathcal{F}\{\mathbf{n}_{nz}\} \cdot \mathcal{F}\{\mathbf{n}_{nz}\}^H \mathbf{F}_L^H] \;=\; \mathbf{F}_L \cdot \hat{\mathbf{K}} \cdot \mathbf{F}_L^H, \qquad (3.22)$$

where $\hat{\mathbf{K}}$ is an $N \times N$ noise covariance matrix consisting of only noise data from the used carrier frequencies and N denotes the number of used carrier frequencies. The dimensions of $\mathbf{F}_L$ are $M \times N$, where M denotes the total number of possible carrier frequencies. Therefore, according to (3.22), $rank\,(\mathbf{K}) \leq N$ because $rank\left(\hat{\mathbf{K}}\right) = N$. Since $N = M - K$, $\mathbf{K}$ does not have full rank which makes $\mathbf{K}$ non-invertible.

3.1.4.2 Invertible, Reduced Noise Covariance Matrix. Fig. 3.11 shows a system with $N = K$, each null-tone occupying the odd carrier frequencies, and $M = 2N$. This is the case when the last half of an 8×8 Hadamard matrix is used to construct the transmission vector, $\mathbf{v}$, when the users, $J \leq 4$. When the first half of an 8×8 Hadamard matrix is used when the users, $J = 4$, the null-tones will occupy the even carrier frequencies. Please refer to the frequency-domain characteristics of a Hadamard matrix shown in Fig. 3.2 and Fig. 3.3.

Fig. 3.11 demonstrates null-tones in $\mathcal{F}\{\mathbf{y}\}$ create linearly dependent terms in $\mathbf{y}$, where $\mathbf{y}_{1:N} = -\mathbf{y}_{(N+1):M}$. Due to (3.8), this also makes $\mathbf{n}_{1:N} = -\mathbf{n}_{(N+1):M}$. Since $\mathbf{K} = E[\mathbf{n}\ \mathbf{n}^T]$, a system similar to Fig. 3.11 with $N = K$, $\mathbf{n}$ will force $\mathbf{K}$ to be

34

Figure 3.12:   As shown in (3.20) and (3.21), null-tones diminish the rank of the noise covariance matrix, $\mathbf{K}$, making it non-invertible. $\mathbf{K}$ shown is a result of null-tones depicted in Fig. 3.11, where $N = K = 4$.

composed of four equal sub-matrices, as shown in Fig. 3.12, which is non-invertible due to its rank [17]. One option to make an invertible $\mathbf{K}$ out of a non-invertible $\mathbf{K}$ is to use a reduced form of $\mathbf{K}$, that is $\mathbf{K}_{red}$. $\mathbf{K}_{red}$ is also defined by (3.22), but will originate with $\mathbf{n}$ using a reduced form, $\mathbf{n}_{red}$. $\mathbf{n}_{red}$ is defined as

$$\mathbf{n}_{red} = \mathbf{n}_{1:N}. \tag{3.23}$$

Using $\mathbf{n}_{red}$ produces $\mathbf{K}_{red}$ that is defined as

$$\mathbf{K}_{red} = E[\mathbf{n}_{red}\ \mathbf{n}_{red}^{H}], \tag{3.24}$$

where $\mathbf{K}_{red}$ is a $N \times N$ matrix with a rank $= N$. Therefore, $\mathbf{K}_{red}$ is invertible.

3.1.4.3   Reduced Received Signal Vector and Reduced Hadamard Codes.

The utilization of an invertible $\mathbf{K}_{red}$ in (3.19) forces the requirement of reduced forms for the received signal vector, $\mathbf{y}$, and individual Hadamard codes, $\mathbf{h}_n$. Fig. 3.11 depicts an equalized, time-domain received signal, $\mathbf{y}$, multiplied with a Hadamard code, $\mathbf{h}_n$. Since the multiplication of the first halves of both $\mathbf{y}$ and $\mathbf{h}_n$ produce the same result as the multiplication of the last halves of both $\mathbf{y}$ and $\mathbf{h}_n$, the reduced terms $\mathbf{y}_{red}$ and $\mathbf{h}_{n,red}$ are respectfully defined as

$$\mathbf{y}_{red} = \mathbf{y}_{1:N}, \tag{3.25}$$

and

$$\mathbf{h}_{n,red} = \mathbf{h}_{n_{1:N}}. \tag{3.26}$$

Now we shall define $a^*_{k,red} = \mathbf{h}^T_{k,red}\mathbf{K}^{-1}_{red}\mathbf{y}_{red}$, $b_{k,red} = \mathbf{h}^T_{k,red}\mathbf{K}^{-1}_{red}\mathbf{h}_{k,red}$, and $c_{kn,red} = \mathbf{h}^T_{k,red}\mathbf{K}^{-1}_{red}\left(\sum^J_{n\neq k}u_n\mathbf{h}_{n,red}\right)$. Substituting the a_k, b_k, and c_{kn} terms from (3.19) with $a^*_{k,red}$, $b_{k,red}$, and $c_{kn,red}$, respectively, results in

$$\tilde{u}_{k,ML} = \frac{\left(a^*_{k,red} - c_{kn,red}\right)}{b_{k,red}} = \frac{\mathbf{h}^T_{k,red}\mathbf{K}^{-1}_{red}\mathbf{y}_{red} - \mathbf{h}^T_{k,red}\mathbf{K}^{-1}_{red}\left(\sum^J_{n\neq k}u_n\mathbf{h}_{n,red}\right)}{\mathbf{h}^T_{k,red}\mathbf{K}^{-1}_{red}\mathbf{h}_{k,red}}$$

$$\boxed{\tilde{u}_{k,ML} = \frac{\mathbf{h}^T_{k,red}\mathbf{K}^{-1}_{red}\left(\mathbf{y}_{red} - \sum^J_{n\neq k}u_n\mathbf{h}_{n,red}\right)}{\mathbf{h}^T_{k,red}\mathbf{K}^{-1}_{red}\mathbf{h}_{k,red}}}. \tag{3.27}$$

(3.27) is the optimal estimate of an individual user's transmitted data, with respect to MLE techniques. Note that $\tilde{u}_{k,ML}$ requires a-priori knowledge of all the other users' 4-QAM data, $u_{n,n\neq k}$, which will be addressed in section 3.1.4.4.

3.1.4.4 Scalar Approximate Maximum Likelihood Estimation. The other users' 4-QAM data, $u_{n,n\neq k}$, in (3.27) requires a-priori knowledge of $u_{n,n\neq k}$, which is not possible to estimate in the maximum-likelihood (ML) sense because a ML estimation (MLE) of $u_{n,n\neq k}$ will also require a-priori knowledge of the other users' 4-QAM data. Therefore, an initial approximate MLE must be acquired for $u_{n,n\neq k}$, which will be denoted as $\tilde{u}_n$ and will be defined as

$$\tilde{u}_n = \frac{\mathbf{h}^T_{n,red}\mathbf{K}^{-1}_{red}\mathbf{y}_{red}}{\mathbf{h}^T_{n,red}\mathbf{K}^{-1}_{red}\mathbf{h}_{n,red}}. \tag{3.28}$$

Note that $\tilde{u}_n$ in (3.28) *is* $\tilde{u}_{k,ML}$ in (3.27), with the exception of the $\sum_{n \neq k}^{J} u_n \mathbf{h}_{n,red}$ term. (3.28) provides an estimate as close as possible to a MLE of $u_{n,n \neq k}$ due to the lack of a-priori knowledge (essentially, ignore other users, which are nearly orthogonal anyway). Using the decision function defined by (3.39) in section 3.1.6, $w(\tilde{u}_n) = \hat{u}_n$, and inserting its result into (3.27) results in $\tilde{u}_{k,ML}$ becoming

$$\boxed{\tilde{u}_{k,ML} = \frac{\mathbf{h}_{k,red}^T \mathbf{K}_{red}^{-1} \left(\mathbf{y}_{red} - \sum_{n \neq k}^{J} \hat{u}_n \mathbf{h}_{n,red} \right)}{\mathbf{h}_{k,red}^T \mathbf{K}_{red}^{-1} \mathbf{h}_{k,red}}}. \tag{3.29}$$

3.1.5   Vector Maximum-Likelihood Estimation.   An alternative estimation approach is to estimate all of the received data at once, instead of estimating the received data on a per user basis as described in (3.29). Proceeding with this approach, the distribution of the received data remains as defined in (3.10). Therefore, (3.11) still holds true and the MLE of the transmitted vector as a whole will be calculated, which is defined as

$$\tilde{\mathbf{u}}_{ML}(\mathbf{y}|\mathbf{v}) = \begin{bmatrix} \tilde{u}_1 \\ \tilde{u}_2 \\ \vdots \\ \tilde{u}_J \end{bmatrix} = \arg \max_{\mathbf{u}} \ln p(\mathbf{y}|\mathbf{v}), \tag{3.30}$$

which becomes

$$\tilde{\mathbf{u}}_{ML}(\mathbf{y}|\mathbf{v}) = \arg \min_{\mathbf{u}} (\mathbf{y} - \sum_{n=1}^{J} u_n \mathbf{h}_n)^H \mathbf{K}^{-1} (\mathbf{y} - \sum_{n=1}^{J} u_n \mathbf{h}_n). \tag{3.31}$$

In (3.31), $\sum_{n=1}^{J} u_n \mathbf{h}_n$ can alternatively be represented as

$$v = Hu = \underbrace{\left[\ \mathbf{h}_1 \mid \mathbf{h}_2 \mid \ldots \mid \mathbf{h}_J\ \right]}_{\mathbf{H}_{M \times J}} \underbrace{\begin{bmatrix} u_1 \\ u_2 \\ \vdots \\ u_J \end{bmatrix}}_{\mathbf{u}_{J \times 1}}. \tag{3.32}$$

(3.31) becomes

$$\tilde{\mathbf{u}}_{ML}(\mathbf{y}|\mathbf{v}) = \arg \min_{\mathbf{u}} \underbrace{(\mathbf{y} - \mathbf{Hu})^H \ \mathbf{K}^{-1} \ (\mathbf{y} - \mathbf{Hu})}_{L} = \arg \min_{\mathbf{u}} \ L. \tag{3.33}$$

In order to determine the minimum of (3.33) we will set the gradient equal to zero

$$\nabla_{\mathbf{u}} L = 0. \tag{3.34}$$

Since $\mathbf{H}$ is real, $\mathbf{H}^* = \mathbf{H}$, and (3.34) becomes

$$\nabla_{\mathbf{u}} \left(\mathbf{y}^H \mathbf{K}^{-1} \mathbf{y} - \mathbf{y}^H \mathbf{K}^{-1} \mathbf{Hu} - (\mathbf{Hu})^H \mathbf{K}^{-1} \mathbf{y} - (\mathbf{Hu})^H \mathbf{K}^{-1} \mathbf{Hu} \right) = 0,$$

$$\nabla_{\mathbf{u}} \left(\mathbf{y}^H \mathbf{K}^{-1} \mathbf{y} - \mathbf{y}^H \mathbf{K}^{-1} \mathbf{Hu} - \mathbf{u}^H \mathbf{H}^T \mathbf{K}^{-1} \mathbf{y} - \mathbf{u}^H \mathbf{H}^T \mathbf{K}^{-1} \mathbf{Hu} \right) = 0. \tag{3.35}$$

(3.35) can be cleaned up by defining $\mathbf{d}^H = \mathbf{y}^H \mathbf{K}^{-1} \mathbf{H}$, $\mathbf{d} = \mathbf{H}^T \mathbf{K}^{-1} \mathbf{y}$, and $\mathbf{e} = \mathbf{H}^T \mathbf{K}^{-1} \mathbf{H}$. Proceeding with these definitions [1, 4]

$$\nabla_{\mathbf{u}} \left(-\mathbf{d}^H \mathbf{u} - \mathbf{u}^H \mathbf{d} - \mathbf{u}^H \mathbf{e} \mathbf{u} \right) = 0,$$

$$\mathbf{0} - 2\mathbf{d} - 2\mathbf{e}\mathbf{u} = 0,$$

$$\tilde{\mathbf{u}}_{ML} = \mathbf{e}^{-1}\mathbf{d},$$

$$\boxed{\tilde{\mathbf{u}}_{ML} = \left(\mathbf{H}^T \mathbf{K}^{-1} \mathbf{H} \right)^{-1} \left(\mathbf{H}^T \mathbf{K}^{-1} \mathbf{y} \right)}. \tag{3.36}$$

$\tilde{\mathbf{u}}_{ML}$ in (3.36) is the vector MLE of all users' modulated data and requires $\mathbf{K}$ to be invertible, therefore we will proceed with reduced forms of $\mathbf{H}$, $\mathbf{K}$, and $\mathbf{y}$ as in section 3.1.4.2 and section 3.1.4.3, resulting in

$$\boxed{\tilde{\mathbf{u}}_{ML} = \left(\mathbf{H}_{red}^T \mathbf{K}_{red}^{-1} \mathbf{H}_{red} \right)^{-1} \left(\mathbf{H}_{red}^T \mathbf{K}_{red}^{-1} \mathbf{y}_{red} \right)}. \tag{3.37}$$

3.1.6 Post-Estimation Decision Function. The output of the receiver's estimators, $\tilde{u}_n$, $\tilde{u}_{k,ML}$, and $\tilde{\mathbf{u}}_{ML}$ will not be exact 4-QAM symbols ($\pm 1 \pm j$) because of signal degradation due to noise. Therefore, directly proceeding each of the system's three estimators, $\tilde{u}_n$, $\tilde{u}_{k,ML}$, and $\tilde{\mathbf{u}}_{k,ML}$, Bayesian hypothesis tests [11] will determine exact 4-QAM symbols based on the test statistics, z or $\mathbf{z}$, where z is either $\tilde{u}_n$ or $\tilde{u}_{k,ML}$, and the vector estimation test statistic, $\mathbf{z}$, is $\tilde{\mathbf{u}}_{k,ML}$.

Since the four values of the possible 4-QAM symbols transmitted are $\pm 1 \pm j$, the hypothesis testing for the test statistic will be either +1 or -1 for both, real and imaginary parts. Therefore, the likelihood-ratio test becomes

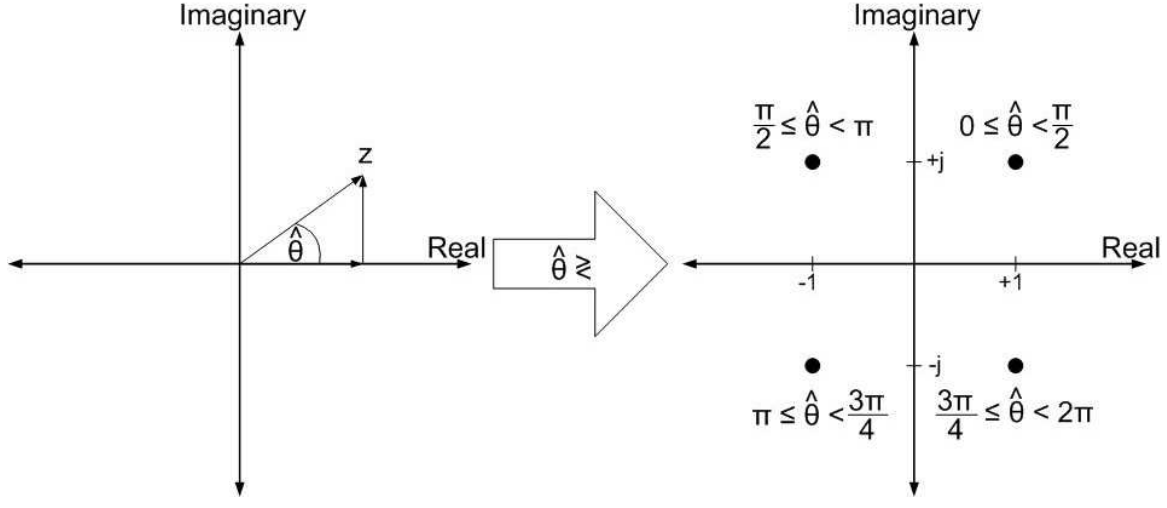$$z \underset{H_1}{\overset{H_0}{\gtrless}} 0. \tag{3.38}$$

Figure 3.13: The angle between the real and imaginary parts of z determine $\hat{\theta}$, and $\hat{\theta}$ is used to determine the received 4-QAM symbol.

(3.38) uses the real and imaginary axes as hypotheses decision boundaries to determine the Bayesian optimal 4-QAM symbol received. The real and imaginary axes as hypotheses decision boundaries can also be interpreted as the angle between the real and imaginary parts of z. Therefore, a demodulator similar to [14] was used to determine the received 4-QAM symbol. i.e., $\text{sign}\{\text{Real}\{z\}\} + j\,\text{sign}\{\text{Imag}\{z\}\}$.

Since $\tilde{u}_n$, $\tilde{u}_{k,ML}$, and $\tilde{\mathbf{u}}_{k,ML}$ are complex, the angle between the real and imaginary parts will be defined as $\hat{\theta}$, and will be used to decide if $\hat{u}_n$, $\hat{u}_{k,ML}$, and each component of $\tilde{\mathbf{u}}_{k,ML}$ are $\pm 1 \pm j$. As shown in Fig. 3.13, the output of the 4-QAM decision function, w, when $z = \tilde{u}_n$ is entered produces

$$w\left(\tilde{u}_n\right) = \hat{u}_n. \tag{3.39}$$

Also, the output of the 4-QAM decision function when $z = \tilde{u}_{k,ML}$ is entered produces

$$w\left(\tilde{u}_{k,ML}\right) = \hat{u}_{k,ML}. \tag{3.40}$$

40
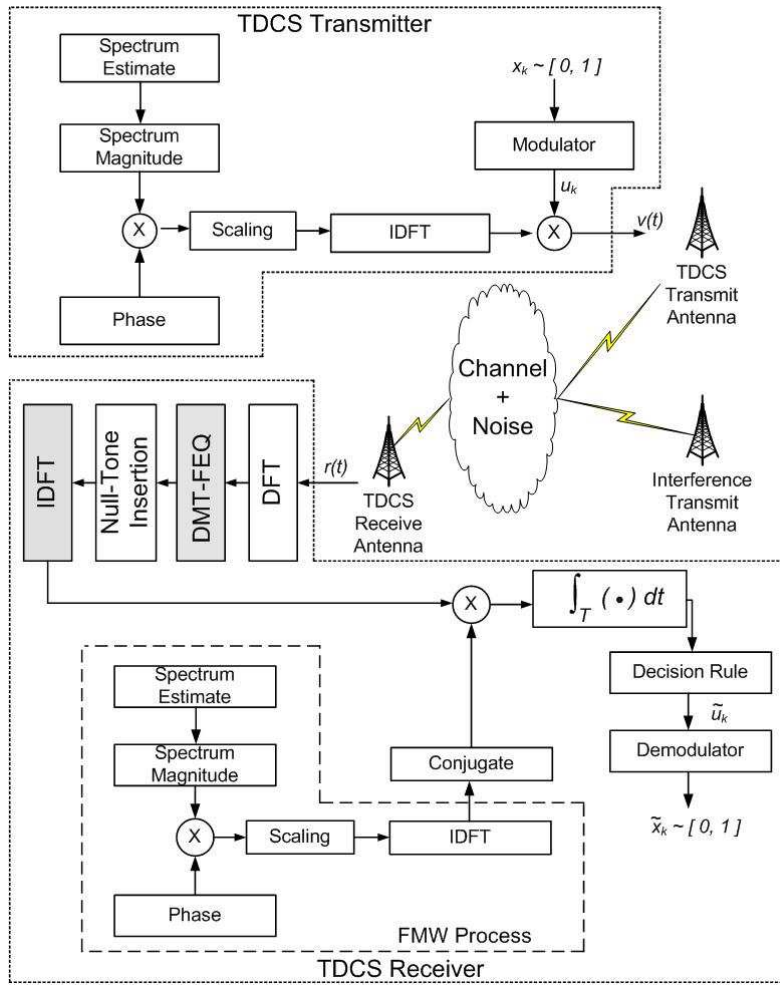
Figure 3.14:   A complete view of the TDCS model.

Finally, the decision function produces the following result when (3.36) is entered to obtain

$$w\left(\tilde{\mathbf{u}}_{ML}\right) = \hat{\mathbf{u}}_{ML},\tag{3.41}$$

where the decision function $w(\mathbf{z})$ in (3.41) acts on the vector $\tilde{\mathbf{u}}_{ML}$ element by element.

3.2   TDCS with DMT-FEQ

Fig. 3.14 illustrates a TDCS system model that has inherent null-tones which can be exploited by using DMT-FEQ. Several TDCS models were used in conjunction

41

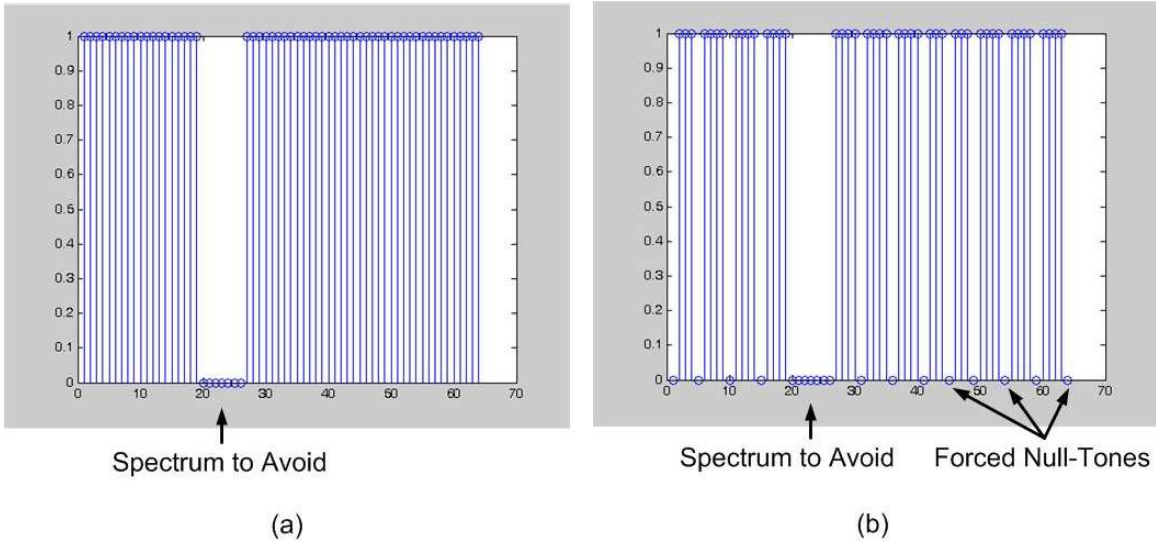Figure 3.15: Two different types of TDCS spectral masks. (a) A traditional TDCS spectral mask containing consecutive null-tones only in the frequency spectrum to avoid. (b) The modified spectral mask contains consecutive null-tones in the frequency spectrum to avoid and additional forced null-tones to maintain compatibility with DMT-FEQ requirements.

with DMT-FEQ to try and identify causes of incompatibility between DMT-FEQ and a traditional TDCS. The TDCS generally possesses all pseudo-random phases and a spectral mask that only contains null-tones in the frequency spectrum to be avoided.

As shown in Fig. 3.14, there are two major variables in a TDCS system model that can be modified for compatibility purposes to make a TDCS system mesh well with DMT-FEQ: phase and spectrum magnitude. Therefore, the phase portion of TDCS was modeled two different ways: conjugate-symmetric phase and pseudo-random phase. The spectrum magnitude portion of TDCS was modeled with a slight modification to a traditional TDCS spectral mask that included forced null-tones. All of these variables are described below.

3.2.1 Conjugate-Symmetric Phase. As described in [10], a conjugate-symmetric sequence was produced for the TDCS phase as follows

$$\theta = \begin{bmatrix} 0 & \theta_1 & \theta_2 & \ldots & \theta_{\frac{M}{2}} & \bigg| & 0 & \theta^*_{\frac{M}{2}} & \ldots & \theta^*_2 & \theta^*_1 \end{bmatrix}^T, \qquad (3.42)$$

where $M = 64$ is the total number of carrier frequencies and θ are uniformly distributed PNs ranging over 0 to 2π. Note that $\frac{M}{2} - 1$ of the possible M phases are PN, rather than the required M PN phases noted in [2].

3.2.2   Pseudo-Random Phase.   The pseudo-random TDCS phase was just that, random phase values ranging from 0 to 2π for all the possible M phases.

3.2.3   Forced Null-Tones Spectrum Mask.   The spectral mask in a traditional TDCS is created for the sole purpose of avoiding a specific frequency range, represented in Fig. 3.15 as the consecutive null-tones. The forced null-tones spectral mask is a slight modification to the traditional TDCS spectral mask and includes additional forced null-tones throughout the frequency spectrum to comply with the equidistant null-tone rule. The additional null-tones are added without violating the null-tone rules noted in Section 3.1.1 [20–22]: Case one is $K \geq L_c - 1, L_c - 1 < 2N$,and Case two is $K \geq 2N, L_c - 1 \geq 2N$. Both spectral masks are shown in Fig. 3.15.

43

IV. Simulation Results

This chapter describes simulation results of equalizing the CDMA and TDCS communications systems described in Sections 3.1 and 3.2 with the discrete-multitone (DMT) frequency-domain equalizer (FEQ) described in [20–22]. To more accurately describe the requirement for channel equalization, this chapter is partitioned into three sections. The first section simulates the Hadamard encoded CDMA communications system transmitting/receiving through an ideal channel without DMT-FEQ, the second section simulates the Hadamard encoded CDMA communications system transmitting/receiving through a non-ideal channel without DMT-FEQ, and the third section simulates both communications systems transmitting/receiving through their respective non-ideal channels with DMT-FEQ employed. Because the requirement for equalization was demonstrated with the Hadamard encoded CDMA simulations, the TDCS simulations were only conducted through a non-ideal channel in conjunction with the DMT-FEQ. A diagram of the simulations performed in this chapter is shown in Fig. 4.1.

The non-ideal channel impulse response (CIR) data was obtained from finite impulse response models of digital microwave radio CIRs in [5]. The initial length of this non-ideal CIR data was $L_c = 300$. The channel windowing process placed the peak channel coefficient in the center. Then 16 channel coefficients were retained before and after the peak coefficient for the Hadamard encoded CDMA system and three were retained before and after the peak coefficient for the TDCS. All other channel coefficients were then removed. The shortened non-ideal channel length was set to the threshold of the null-tone rules, where $L_c = 33$ for Hadamard encoded CDMA simulations and $L_c = 7$ for the TDCS simulations.

The Hadamard encoded CDMA simulations followed the system models described in Section 3.1 and were comprised of combinations of correctly chosen Hadamard codes that did not violate the null-tone conditions noted in Section 3.1.1. The size of the Hadamard matrix used was 64×64. The noise used in simulations involving the first half of the Hadamard spreading codes, $\mathbf{h}_{1:32}$, was assumed to be zero-mean
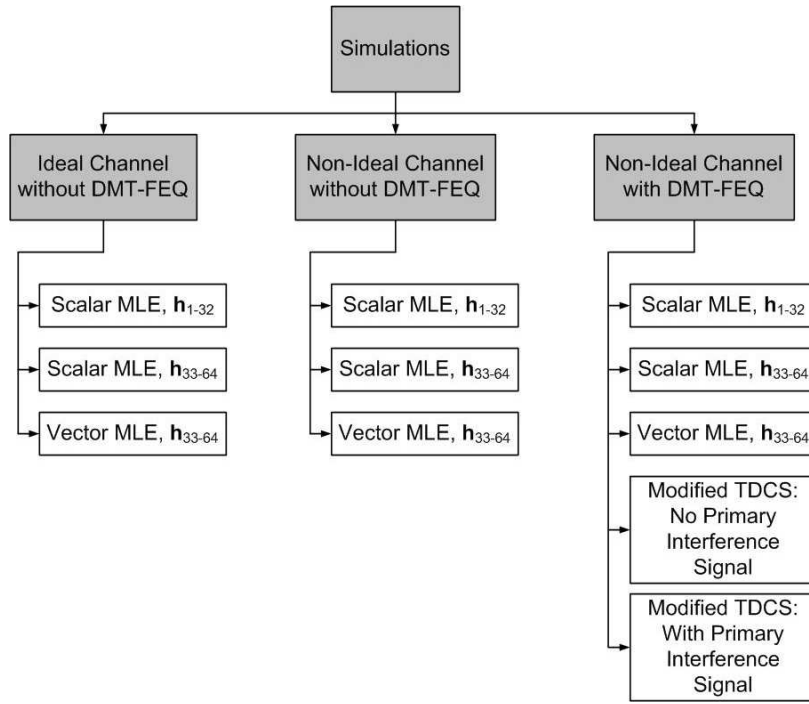
Figure 4.1:   A diagram of simulations conducted.

with unit variance in order to construct an invertible noise covariance matrix. Also, only $\mathbf{h}_{33:64}$ were used in conjunction with the vector estimator because $\mathbf{h}_{1:32}$ led to poor performance when used in a Hadamard encoded CDMA communications system utilizing DMT-FEQ.

TDCS simulations followed the system models described in Section 3.2, where only one TDCS user was using the system's available bandwidth. The TDCS simulations were split into two categories: simulations without a primary interference signal and simulations with a primary interference signal. Although a portion of the frequency spectrum was restricted from use, there were no primary users transmitting on the simulated interference frequencies represented in Fig. 3.15(a) as the consecutive zeros during the initial TDCS simulations. These initial TDCS simulations were conducted for the sole purpose of identifying TDCS properties that worked well with DMT-FEQ. The simulations with a primary interference signal were used to validate the findings from the initial simulations in a more realistic TDCS model. Also, because the requirement for equalization was demonstrated with the Hadamard encoded
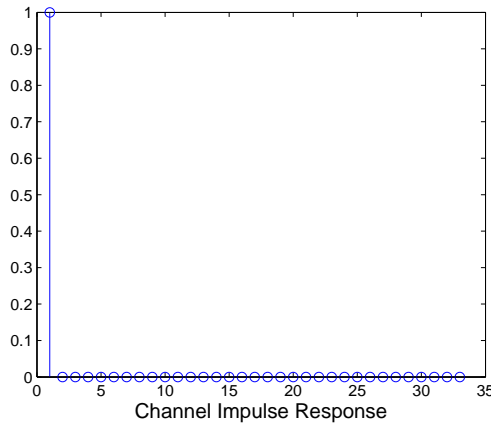
Figure 4.2:   Ideal CIR for Hadamard simulations. $L_c = 33$.

CDMA simulations, the TDCS simulations were only conducted through a non-ideal channel in conjunction with DMT-FEQ.

All simulations had additive white Gaussian noise (AWGN) injected into the receiver input, where the received signal to noise ratio (SNR_{Rx}) ranged from 0dB to 40dB. The Hadamard encoded CDMA simulations' SNR_{Rx} was in 5dB increments and the TDCS simulations' SNR_{Rx} was in 1dB increments.

All simulations had each user transmit and receive 30,400 of their respective 4-QAM symbols, or, on the binary level, each user transmitted and received 60,800 of their respective binary data bits.

4.1   Ideal Channel without DMT-FEQ

Since most communication systems operate over channels that are non-ideal, the results in this section are used as a baseline for the subsequent simulation results that model more realistic environments for a Hadamard encoded CDMA communications system.

The Hadamard encoded CDMA system is shown in Fig. 3.1, where the only exception was that the DFT, DMT-FEQ, null-tone insertion, and the IDFT were not used. The number of synchronous users, $J = 1, 2, 4, 8, 16$, and 32. The ideal channel impulse response (CIR) in these simulations is of length, $L_c = 33$, as shown in Fig.
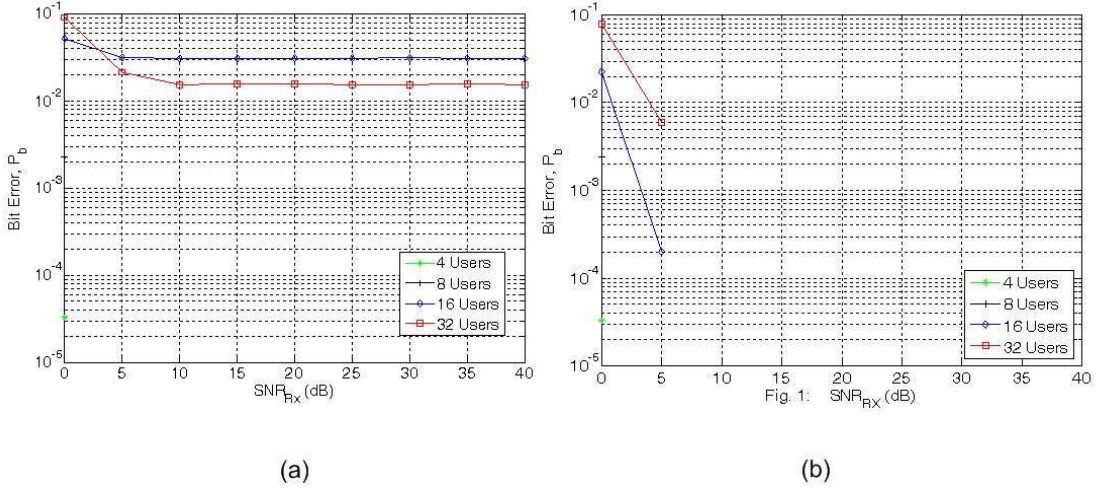
46

Figure 4.3: P_b vs. SNR_{Rx} results for a Hadamard encoded CDMA communications system with an ideal CIR, not using the DMT-FEQ, and using the scalar estimator. (a) $\mathbf{h}_{1:32}$ were used. (b) $\mathbf{h}_{33:64}$ were used.

4.2. Although $L_c = 33$ in Fig. 4.2, zero signal delay and zero signal distortion will occur when a signal is applied to the ideal CIR.

4.1.1   Scalar MLE, $\mathbf{h}_{1:32}$.   Although an ideal CIR was used, the probability of bit error, P_b, versus SNR_{Rx} results in Fig. 4.3(a) indicate high bit error rates when a CDMA system accommodates 16 or more synchronous users when $\mathbf{h}_{1:32}$ was used.

4.1.2   Scalar MLE, $\mathbf{h}_{33:64}$.   Unlike the P_b versus SNR_{Rx} results in Fig. 4.3(a), the results in Fig. 4.3(b) show P_b improvement as SNR_{Rx} increases. Therefore, these results suggest case one or case two and the equidistant null-tone rules must be adhered to for proper equalization by DMT-FEQ.

4.1.3   Vector MLE, $\mathbf{h}_{33:64}$.   Results from using the vector estimation are shown in Fig. 4.4.
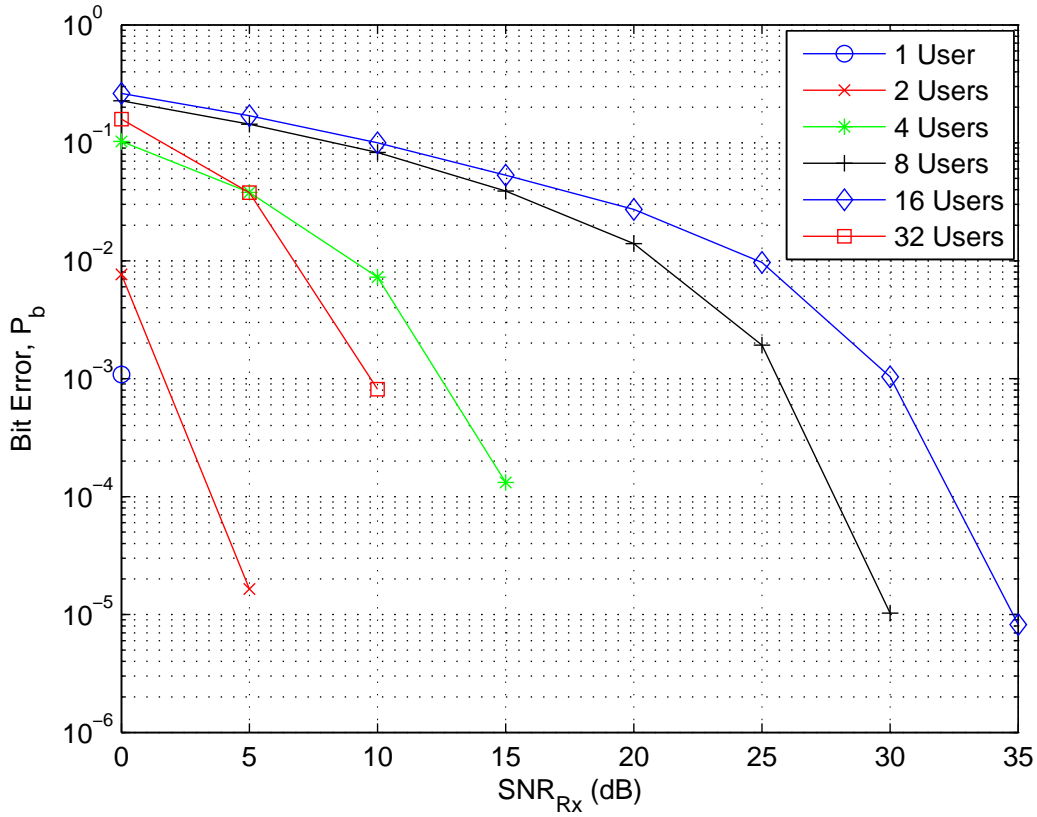
47

Figure 4.4: P_b vs. SNR_{Rx} results for Hadamard encoded CDMA communications system with with an ideal CIR, no DMT-FEQ, and using the vector estimator. $\mathbf{h}_{33:64}$ were used.

4.2 Non-Ideal Channel without DMT-FEQ

Many, if not all, fielded communications systems are not afforded the luxury of operating through ideal channels. Therefore, this section simulated the Hadamard encoded CDMA communications system operating through a non-ideal channel without utilizing DMT-FEQ and is shown in Fig. 3.1, where the only exception was that the DFT, DMT-FEQ, null-tone insertion, and the IDFT were not used. The CIR used for simulations is shown in Fig. 4.5(a), where the number of users, $J = 1, 2, 4, 8, 16,$ and 32.
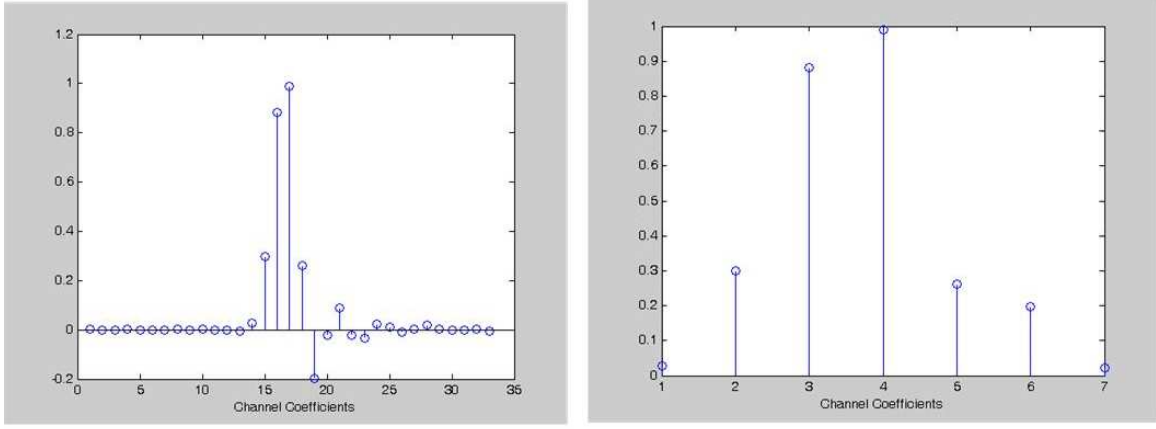
(a)   (b)

Figure 4.5: Non-Ideal CIRs. Original length of CIR was $L_c = 300$ and was obtained from [5]. (a) Non-ideal CIR used for Hadamard simulations shortened to $L_c = 33$ in order to barely satisfy the case one null-tone rule noted in section 3.1.1. (b) Non-ideal CIR used for TDCS simulations shortened to $L_c = 7$.

4.2.1 Scalar MLE, $\mathbf{h}_{1:32}$. The P_b versus SNR_{Rx} results shown in Fig. 4.6(a) reflect the consequences of not equalizing a signal after transmission through a non-ideal channel. The results indicate poorer performance in terms of bit error rate when no equalization was used because P_b increased from an approximate average of 1 in 50, shown in Fig. 4.3(a), to an approximate average of 1 in 5, shown in Fig. 4.6(a).

4.2.2 Scalar MLE, $\mathbf{h}_{33:64}$. The P_b versus SNR_{Rx} results shown in Fig. 4.6(b) also reflect the impact of not equalizing a signal after transmission through a non-ideal channel. The results indicate poorer performance in terms of bit error rate when no equalization was used because P_b increased from the baseline results shown in Fig. 4.3(b) to an approximate average for users $J \geq 4$ of 1 in 5. The increase in P_b due to not utilizing the DMT-FEQ is shown in Fig. 4.6(b).
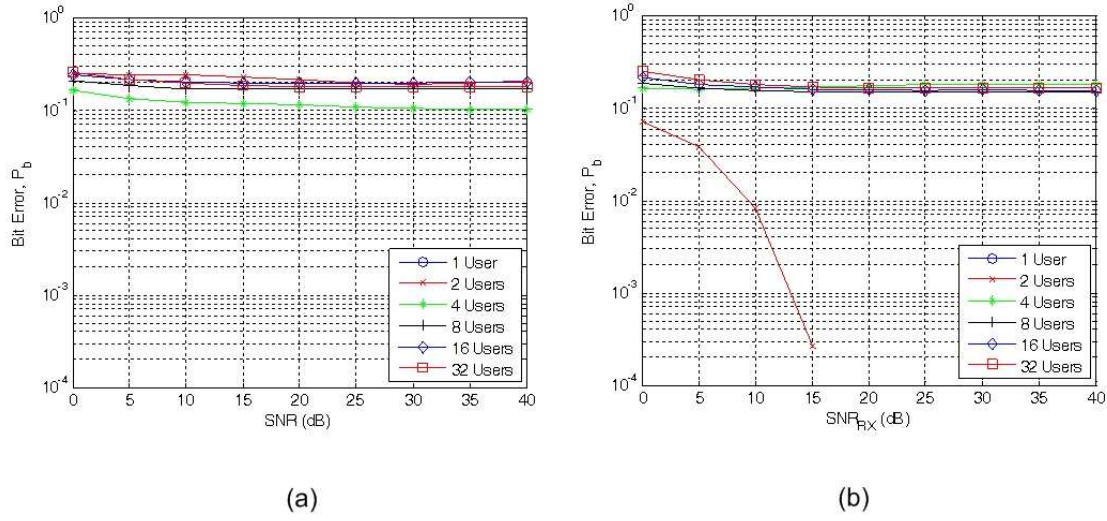
49

Figure 4.6: P_b vs. SNR_{Rx} results for a Hadamard encoded CDMA communications system with a non-ideal CIR, no DMT-FEQ, and using the scalar estimator. (a) $\mathbf{h}_{1:32}$ were used. (b) $\mathbf{h}_{33:64}$ were used.

4.2.3 Vector MLE, $\mathbf{h}_{33:64}$. The P_b versus SNR_{Rx} results shown in Fig. 4.7 illustrates the consequences of not using an equalizer in a Hadamard encoded CDMA communications system operating through a non-ideal channel.

4.3 Non-Ideal Channel with DMT-FEQ

This section simulated the two communications systems, Hadamard encoded CDMA and TDCS, operating through their respective non-ideal channels and utilizing DMT-FEQ. The simulated Hadamard encoded CDMA communications system is shown in Fig. 3.1, where the number of users, $J = 1, 2, 4, 8, 16$, and 32. The channel data used in this section for the Hadamard encoded CDMA communications system was the same channel data that was used in section 4.2, and is shown in Fig. 4.5(a). The channel data used for the TDCS simulations is shown in Fig. 4.5(b).

4.3.1 Scalar Estimator, $\mathbf{h}_{1:32}$. The P_b versus SNR_{Rx} results shown in Fig. 4.8(a) demonstrate improvement over the P_b versus SNR_{Rx} results shown in Fig. 4.6(a).
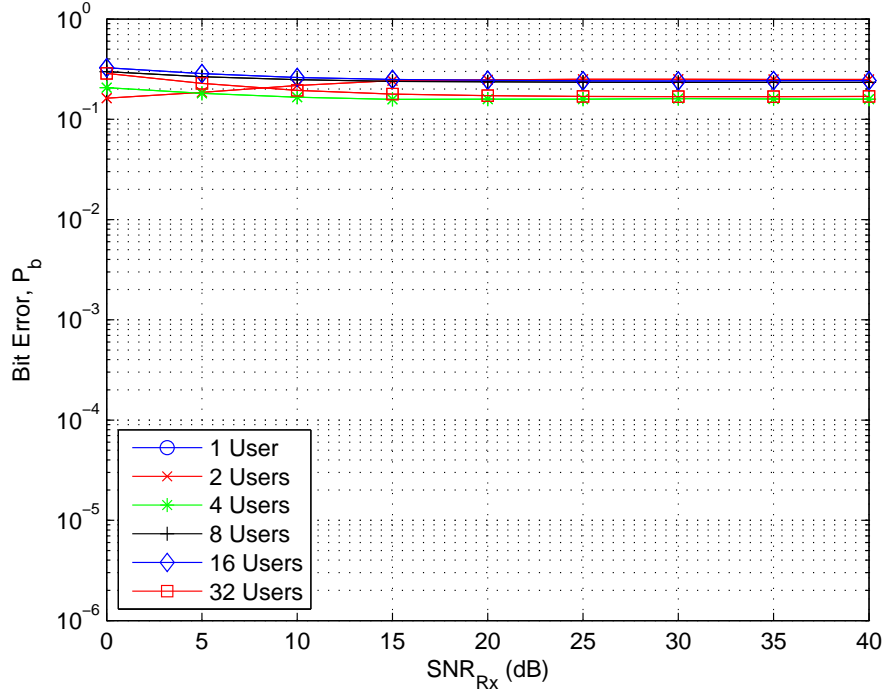
50

Figure 4.7: P_b vs. SNR_{Rx} results for a Hadamard encoded CDMA communications system with a non-ideal CIR, no DMT-FEQ, and using the vector estimator. $\mathbf{h}_{33:64}$ were used.

4.3.2 Scalar Estimator, $\mathbf{h}_{33:64}$. The P_b versus SNR_{Rx} results shown in Fig. 4.8(b) demonstrate improvement for a Hadamard encoded CDMA communications system for all of the number of system users compared with the P_b versus SNR_{Rx} results shown in Fig. 4.6(b).

4.3.3 Vector Estimator, $\mathbf{h}_{33:64}$. The results from using the vector estimator are shown in Fig. 4.9, and are an improvement over the scalar estimator shown in Fig. 4.8(b).

4.3.4 Modified TDCS with No Primary Interference. The simulated TDCS is shown in Fig. 3.14, where the only exception here is that the primary interference transmit antenna was removed. Also, the number of TDCS users, $J = 1$.
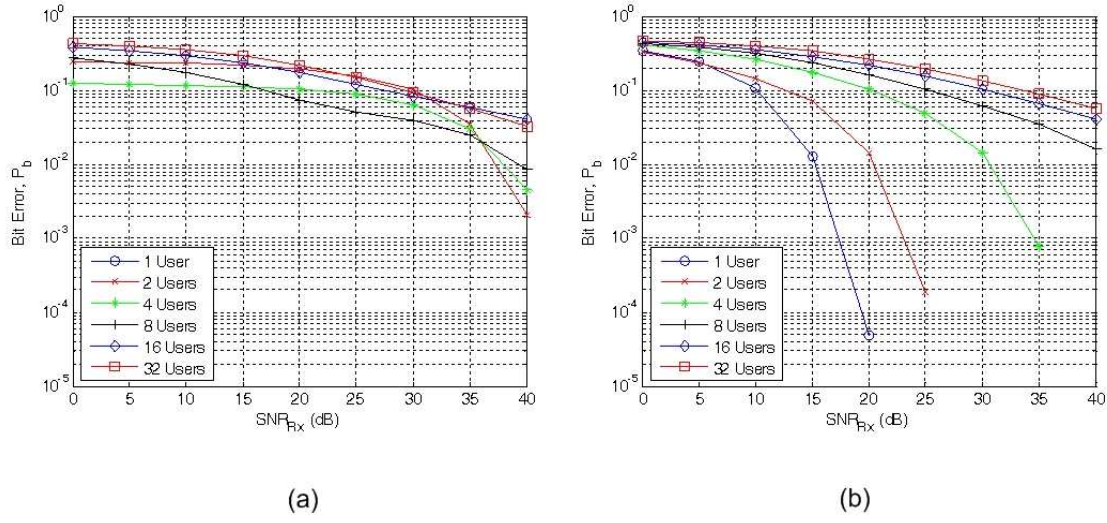
51

Figure 4.8: P_b vs. SNR_{Rx} results for a Hadamard encoded CDMA communications system with with a non-ideal CIR, using DMT-FEQ, and using the scalar estimator. (a) $\mathbf{h}_{1:32}$ were used. (b) $\mathbf{h}_{33:64}$ were used.

The simulation results shown in Fig. 4.10 show that a traditional TDCS does not work well with DMT-FEQ because of the relatively high bit error rates compared with a modified TDCS with conjugate-symmetric phase and a forced null-tones spectral mask. Note that these modifications to TDCS produced better results and retains the required noise-like appearance.

4.3.5   Modified TDCS with Primary Interference.   The simulated TDCS with no primary interference signal is shown in Fig. 3.14, where the number of TDCS users, $J = 1$.

The simulation results shown in Fig. 4.11 show that the system's bit error rates remain consistent regardless of the signal to interference ratio (SIR).
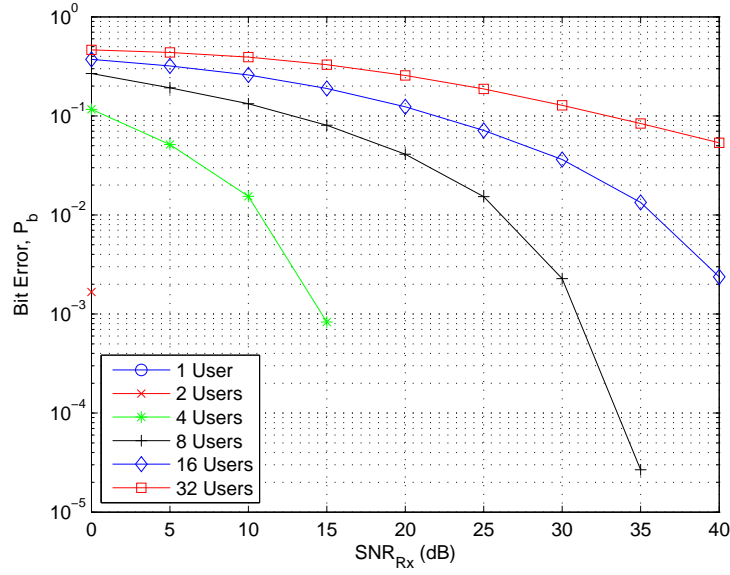
Figure 4.9: P_b vs. SNR_{Rx} results for a Hadamard encoded CDMA communications system with with a non-ideal CIR, using the DMT-FEQ, and using the vector estimator. $\mathbf{h}_{33:64}$ were used.
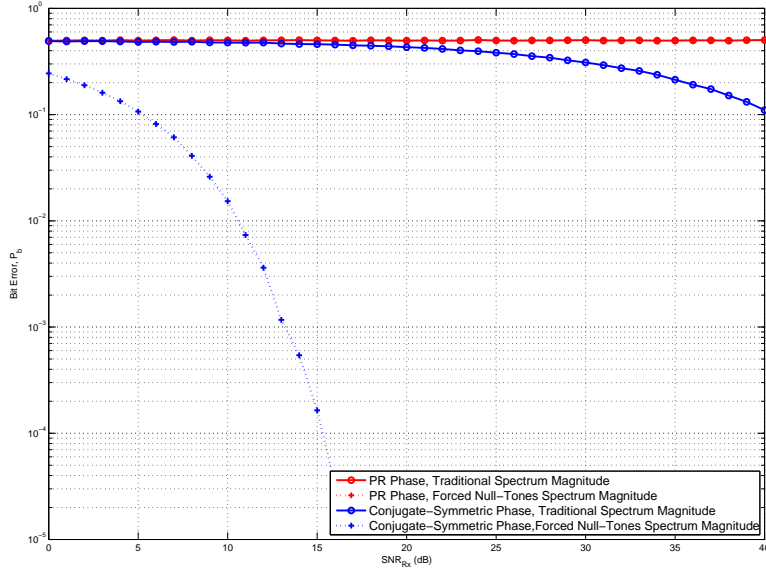

Figure 4.10: TDCS simulation results with a non-ideal CIR, $L_c = 7$, shown in Fig. 4.5(b) and using DMT-FEQ. $J = 1$ user with no primary interference signal.
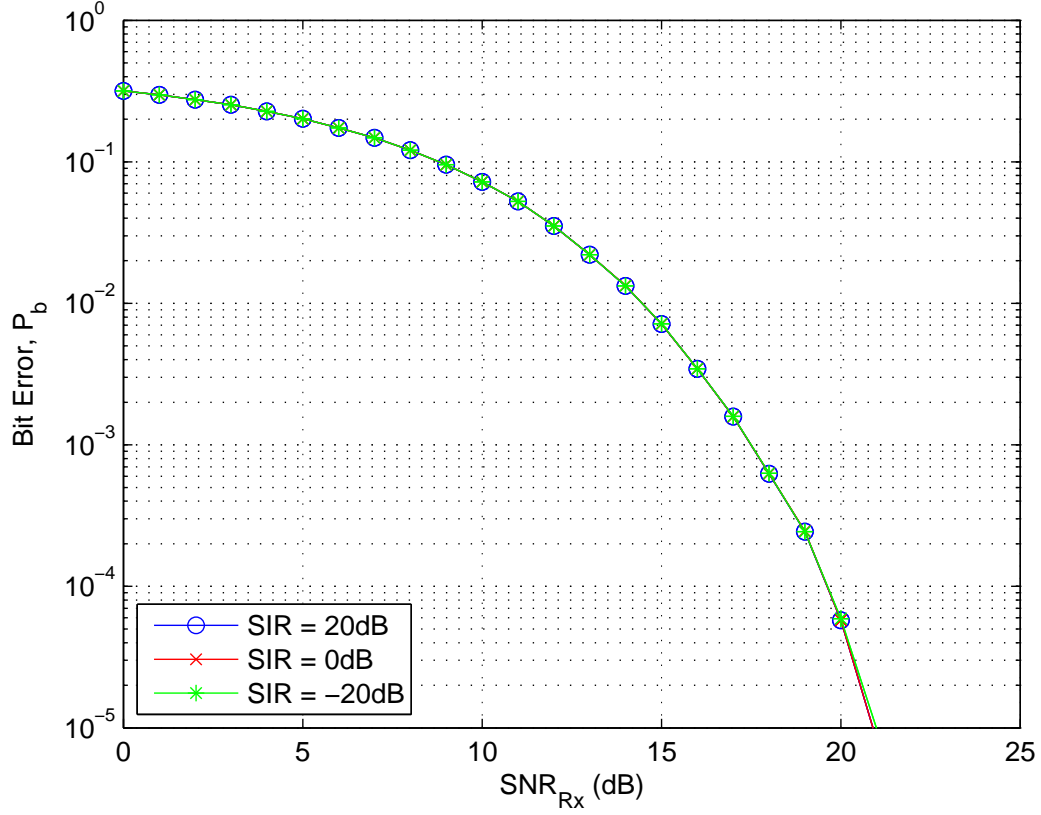
Figure 4.11: Simulation results with a modified TDCS having a conjugate-symmetric phase and forced null-tones spectral mask. Simulations were conducted with the non-ideal CIR shown in Fig. 4.5(b), using DMT-FEQ, $J = 1$ user, and a primary interference signal. The spectral mask used is shown in Fig. 3.15(b).

V. Conclusion

Results from Chapter 4 suggest the discrete multitone frequency-domain equalizer (DMT-FEQ) works best in a multi-user Hadamard encoded CDMA communication system environment when the vector estimation is performed, rather than the scalar estimation. Also, the last half of the available spreading code set produced better performance than the first half of the spreading code set.

The DMT-FEQ may also be suitable for covert applications by modifying the traditional TDCS containing all pseudo-random phases to include only consecutive null-tones in its spectral mask. When using DMT-FEQ with TDCS, simulation results show that modifications to TDCS' phase component to conjugate-symmetric phases and modifications to TDCS' spectrum mask component to include forced null-tones provide acceptable results. This may be a viable alternative given that half of the required phases were assigned as pseudo-random numbers, then were conjugated and mirrored in the remaining half of the required phases, which may preserve the required noise-like appearance of TDCS signals in the time-domain.

Bibliography

1. Brookes, M. *The Matrix Reference Manual.* Online, http://www.ee.ic.ac.uk/hp/staff/dmb/matrix/intro.html.

2. Chakravarthy, J. P. Stephens A. K. Shaw M. A. Temple, A. S. Nunez. "TDCS, OFDM, and MC-CDMA: A Brief Tutorial". *IEEE Communications Magazine*, 50:S11–S15, September 2005.

3. Haker, M. E. *Hardware Realization of a Transform Domain Communication System.* Master's thesis, Graduate School of Engineering and Management, Air Force Institute of Technology (AU), Wright-Patterson AFB OH, March 2007.

4. Haykin, S. *Adaptive Filter Theory.* Prentice Hall, Upper Saddle River, New Jersey 07458, 4 edition, 2002.

5. http://spib.rice.edu/spib/microwave.html. "Microwave Data, chan1.mat (chan1a): T=30Mb". Online, October 2000.

6. Klein, R. W. *Wavelet Domain Communication System (WDCS): Design, Model, Simulation, and Analysis.* Master's thesis, Graduate School of Engineering and Management, Air Force Institute of Technology (AU), Wright-Patterson AFB OH, March 2001.

7. Lindsey, W. C. and M. K. Simon. *Telecommunication Systems Engineering.* Prentice-Hall, Inc., Englewood Cliffs, N.J., 1973.

8. Müller, H. Rohling and R. Grünheid. "Comparison of different Detection Algorithms for OFDM-CDMA in Broadband Rayleigh Fading". *Vehicular Technology Conference*, volume 2, 835 – 838. July 1995.

9. Nunez, A. S. *Interference Suppression in Multiple Access Communications Using M-ary Phase Shift Keying Generated Using Spectral Encoding.* Master's thesis, Graduate School of Engineering and Management, Air Force Institute of Technology (AU), Wright-Patterson AFB OH, March 2004.

10. Oppenheim, J. R. Buck, R. W. Schafer. *Discrete-Time Signal Processing.* Signal Processing Series. Prentice-Hall, 2 edition, 1998.

11. Poor, H. V. *An Introduction to Signal Detection and Estimation.* Springer, 2 edition, 1994. ISBN 0-387-94173-8.

12. Radcliffe, R. A. *Design and Simulation of a Transform Domain Communication System.* Master's thesis, Graduate School of Engineering and Management, Air Force Institute of Technology (AU), Wright-Patterson AFB OH, December 1996.

13. Riddle, D. F. *Calculus and Analytic Geometry.* PWS Publishing Company, 4 edition, 1993.

14. Sklar, B. *Digital Communications: Fundamentals and Applications*. B. Goodwin, 2 edition, 2001. ISBN 0-13-084788-7.

15. Stewart, J. *Calculus Concepts and Contexts*. Brooks/Cole Publishing Company, 1998.

16. Stoica, R. Roses. *Spectral Analysis of Signals*. Pearson Prentice Hall, Upper Saddle River, NJ, 2005.

17. Strang, G. *Linear Algebra and Its Applications*. Thomson, Brooks/Cole, 4 edition, 2006.

18. Stremler, F. G. *Introduction to Communication Systems*. Addison Wesley Longman, 3 edition, 1992.

19. Tomasi, W. *Electronic Communications Systems: Fundamentals Through Advanced*. Prentice-Hall, Inc., 3 edition, 1998.

20. Trautmann and N. J. Fliege. "A New Equalizer for Multitone Systems Without Guard Time". *IEEE Communications Letters*, 6(1):34–36, January 2002.

21. Trautmann and N. J. Fliege. "Perfect Equalization for DMT Systems Without Guard Interval". *IEEE Journal on Selected Areas in Communications*, 20(5):987–996, June 2002.

22. Trautmann, T. Karp and N. Fliege. "Frequency Domain Equalization of DMT/OFDM Systems with Insufficient Guard Interval". volume 3 of *IEEE International Conference on Communications*, 1646–1650. 2002.

23. Viterbi, A. J. "On Coded Phase-Coherent Communications". *IRE Trans. Space Electrom. Telem.*, SET7:3–14, March 1961.

Vita

Captain Alfred A. Tamayo, III graduated from Clovis West High School in Fresno, California in 1996. Shortly thereafter, he attended DeVry University in Phoenix, Arizona and graduated in 1999 with a Bachelor of Science in Electronic Engineering Technology.

After earning his BS, he acquired a position as a manufacturing test engineer for Lam Research, where he ensured the quality of the semiconductor fabrication equipment off the manufacturing line until he entered the U.S. Air Force in March 2002 and was was subsequently commissioned through the USAF Officer Training School at Maxwell AFB, Alabama in May 2002.

His first assignment was to Misawa Air Base, Japan, where he worked in 373d Support Squadron as well as several flights in the 35th Communications Squadron. His second assignment was to the 3d Combat Communications Group where he was a tactical communications and information systems engineer, and was initiated as a proud member of the Wolfpack. While assigned to the 3d Herd, he earned his MBA from University of Phoenix and also deployed to South-West Asia in support of Operation Enduring Freedom and Operation Iraqi Freedom as the assistant theater communications and information systems engineer. In August 2006, he entered the Graduate School of Engineering and Management, Air Force Institute of Technology (AFIT). Upon completion of his Masters Degree at AFIT, Captain Tamayo will be assigned to the Air Force Communications Agency, at Scott AFB, Illinois.

Permanent address: 2950 Hobson Way
Air Force Institute of Technology
Wright-Patterson AFB, OH 45433

REPORT DOCUMENTATION PAGE

Form Approved
OMB No. 0704-0188

1. REPORT DATE (DD-MM-YYYY)	2. REPORT TYPE	3. DATES COVERED (From - To)
27-03-2008	Master's Thesis	August 2006 - March 2008

4. TITLE AND SUBTITLE

Applying Frequency-Domain Equalization to Code-Division Multiple Access and Transform-Domain Communications Systems

5a. CONTRACT NUMBER

5b. GRANT NUMBER

5c. PROGRAM ELEMENT NUMBER

6. AUTHOR(S)

Tamayo, Alfred, A, III., Capt, USAF

5d. PROJECT NUMBER

5e. TASK NUMBER

5f. WORK UNIT NUMBER

7. PERFORMING ORGANIZATION NAME(S) AND ADDRESS(ES)

Air Force Institute of Technology
Graduate School of Engineering and Management (AFIT/EN)
2950 Hobson Way
WPAFB OH 45433-7765

8. PERFORMING ORGANIZATION REPORT NUMBER

AFIT/GE/ENG/08-33

9. SPONSORING/MONITORING AGENCY NAME(S) AND ADDRESS(ES)

AFRL/RYRE
Attn: Mr. Vasu Chakravarthy (AFMC)
2241 Avionics Circle
WPAFB OH 45433 DSN: 785-5579 x 4245
email: vasu.chakravarthy@wpafb.af.mil

10. SPONSOR/MONITOR'S ACRONYM(S)

11. SPONSOR/MONITOR'S REPORT NUMBER(S)

12. DISTRIBUTION/AVAILABILITY STATEMENT

APPROVED FOR PUBLIC RELEASE; DISTRIBUTION UNLIMITED

13. SUPPLEMENTARY NOTES

14. ABSTRACT

This research examined the theory and application of using discrete multi-tone (DMT) frequency-domain equalization (FEQ) with communications systems that inherently possess null-tones in their respective transmission frequencies. DMT-FEQ relies on null-tones to equalize a non-ideal channel. A Hadamard encoded code division multiple access (CDMA) communications system with up to 32 synchronous users and a transform domain communications system (TDCS) with one user were investigated. Both communications systems were simulated while operating with real channel data corrupted by noise. Simulation results showed that the Hadamard encoded CDMA system worked well with DMT-FEQ only when the transmission signal obeyed DMT-FEQ null-tone conditions in conjunction with a vector estimation method. Simulation results also showed that modifications to TDCS with a conjugate-symmetric phase component in conjunction with a modified spectral mask with consecutive null-tones and forced null-tones provided acceptable results when equalizing with DMT-FEQ.

15. SUBJECT TERMS

Code-Division Multiple Access, Transform-Domain Communications System, Orthogonal Frequency-Division Multiplexing, Discrete-Multitone, Frequency-Domain Equalization

16. SECURITY CLASSIFICATION OF:			17. LIMITATION OF ABSTRACT	18. NUMBER OF PAGES	19a. NAME OF RESPONSIBLE PERSON
a. REPORT	b. ABSTRACT	c. THIS PAGE			Richard K. Martin (ENG)
U	U	U	UU	72	19b. TELEPHONE NUMBER (Include area code) (937) 255-3636, x4625; richard.martin@afit.edu

Standard Form 298 (Rev. 8/98)
Prescribed by ANSI Std. Z39.18